IVYSPRING INTERNATIONAL PUBLISHER

Theranostics

2017; 7(18): 4424-4444. doi: 10.7150/thno.18832

Research Paper

Temperature-Sensitive Gold Nanoparticle-Coated Pluronic-PLL Nanoparticles for Drug Delivery and Chemo-Photothermal Therapy

Ying Sun[1]*, Qi Wang[1]*, Jianhua Chen[1], Lei Liu[1], Li Ding[1], Ming Shen[1], Jin Li[3]✉, Baoshan Han[2]✉ and Yourong Duan[1]✉

1. State Key Laboratory of Oncogenes and Related Genes, Shanghai Cancer Institute, Renji Hospital, School of Medicine, Shanghai Jiao Tong University, Shanghai 200032, People's Republic of China;
2. Department of General Surgery, School of Medicine, Xinhua Hospital, Shanghai Jiao Tong University, Shanghai 200092, People's Republic of China;
3. Department of Ophthalmology, Renji Hospital, School of Medicine, Shanghai Jiao Tong University, Shanghai 200127, People's Republic of China.

* These authors contributed equally to this work.

✉ Corresponding authors: Tel.: +86 21 64437139; fax: +86 21 64437139. E-mail: yrduan@shsci.org (Y. Duan). Tel.: +86 21 25078999; fax: +86 21 25078999. E-mail: hanbaosan@126.com (B. Han). Tel.: +86 21 63672937; fax: +86 21 63730455. E-mail: lijinmpa@163.com (J. Li).

Received: 2016.12.19; Accepted: 2017.08.25; Published: 2017.10.06

Abstract

Gold nanoparticle-coated Pluronic-*b*-poly(L-lysine) nanoparticles (Pluronic-PLL@Au NPs) were synthesized via an easy one-step method and employed as carriers for the delivery of paclitaxel (PTX) in chemo-photothermal therapy, in which Pluronic-PLL acts as the reductant for the formation of AuNPs without the need for an additional reducing agent. Methods: The deposition of AuNPs on the surface of Pluronic-PLL micelles and the thermal response of the system were followed via ultraviolet-visible spectroscopy and dynamic light scattering. Calcein-AM and MTT assays were used to study the cell viability of MDA-MB-231 cells treated with PTX-loaded Pluronic-PLL@Au NPs, and we then irradiated the cells with NIR light. Results: An obvious temperature response was observed for the Pluronic-PLL@Au NPs. Blood compatibility and *in vitro* cytotoxicity assays confirmed that the Pluronic-PLL@Au NPs have excellent biocompatibility. Compared to Taxol, the PTX-loaded Pluronic-PLL@Au NPs exhibited higher cytotoxicity in MDA-MB-231 cells. All of these results and confocal laser scanning microscopy analysis results suggest that Pluronic-PLL@Au NPs greatly enhance the cellular uptake efficiency of the drug. Conclusion: As confirmed by *in vitro* and *in vivo* studies, the combination of chemotherapy and photothermal therapy can cause more damage than chemo- or photothermal therapy did alone, demonstrating the synergistic effect of chemo-photothermal treatment. Thus, the as-prepared Pluronic-PLL@Au NPs are promising for chemo-photothermal therapy.

Key words: One-Pot Synthesis; Thermally Sensitive; Gold Nanoparticle; Pluronic-b-poly(L-lysine); Drug Delivery; Chemo-Photothermal.

Introduction

Various polymeric nanoparticles with diverse morphological characteristics are utilized for drug or gene therapy, and their diagnostic applications have attracted significant interest in the past two decades.[1-4] Among these nanoparticles, copolymer nanoparticles with responses to stimuli have attracted growing attention due to their diverse self-assembly behavior in response to various stimuli, such as temperature, light and pH. Compared with other polymer carriers, Pluronic copolymers have been widely used in pharmaceutical preparations.[5,6] However, it is well established that Pluronic copolymers self-assemble into micelles with a PPO-rich core and a PEO-rich corona when the concentration of the Pluronic

copolymer is above the critical micelle concentration (CMC).[7] Moreover, due to a lack of functional groups, the use of Pluronic micelles is limited in bio-material applications. Recently, many investigations have attempted to improve the stability of Pluronic micelles and create Pluronic micelles with functional groups. Poly(L-lysine) (PLL) is a very important biological macromolecule for biomedical applications, displaying a relatively high cationic surface charge and excellent biocompatibility and biodegradability.[8] Due to its hydrosolubility and functional NH_2 side groups, the cationic copolymer (PLL) could improve the affinity of Pluronic micelles towards cells or combinations with drugs, antibodies or DNA. Positively charged PLL can be used to synthesize gold nanoparticles (AuNPs) that act as a reductant without the need for an external reducing agent,[9] which provides a "green" method for nanoparticle preparation. AuNPs have attracted substantial interest during the past decade for their potential applications in optics, electronics, chemical sensing, catalysis, molecular diagnostics and biosensors.[10-13] As a promising nanobiomaterial, Au nanoscale particles show efficient local heating upon excitation of surface plasmon oscillations and have been widely studied as photothermal agents for cancer therapy,[14-16] as traditional hyperthermia treatments typically lack specificity for the tumor.[17,18] Chemo-photothermal therapy provides a convenient and efficient way to combine the advantages of chemo- and thermal therapeutic effects. Huiyul Park et al. developed drug-loaded poly(lactic-co-glycolic acid)-Au half-shell nanoparticles for the tumor-specific delivery of heat and drugs[15] these particles were prepared by spin-casting aqueous suspensions of NPs onto a silicon substrate. Because the physical deposition method yields half-shells, the drug is released through the open half of the shell, the interior of which is now exposed.

In this paper, a novel Pluronic-*b*-poly(L-lysine) (Pluronic-PLL) block copolymer was synthesized with Pluronic-NH_2 through the ring-opening polymerization (ROP) of the amino acid L-lysine *N*-carboxyanhydride (NCA). Drug-loaded gold nanoparticle-coated Pluronic-*b*-poly(L-lysine) nanoparticles (drug-loaded Pluronic-PLL@Au NPs) were synthesized by an easy one-step method and employed as carriers for the delivery of paclitaxel (PTX) in chemo-photothermal therapy. PLL was used as a reducing agent, stabilizing the gold nanoparticles without introducing any environmental toxicity or biological hazards. The drug is encapsulated within Pluronic-PLL micelles, and an Au layer is deposited on these micelles. The Pluronic-PLL@Au NPs were found to have an excellent biocompatibility, presumably due to the biocompatible nature of their two constituent polymers. We studied the therapeutic efficacy of PTX-loaded Pluronic-PLL@Au NPs both in vitro and in vivo with a combination of chemotherapy and photothermal therapy. The chemo-photothermal treatment showed a synergistic effect, resulting in better therapeutic efficacy.

Materials and Methods

Materials

The PEO-PPO-PEO triblock copolymer ($(PEO)_{100}(PPO)_{65}(PEO)_{100}$, Pluronic F127, M_w = 12600) was obtained from BASF Corporation. Rhodamine B (RB) was purchased from Sigma-Aldrich. Chloroauric acid ($HAuCl_4$) was purchased from Acros. *N*,*N*'-dicyclohexylcarbodiimide (DCC) and 4-dimethylamiopryidine (DMAP) were provided by Sinopharm Chemical Reagent Co., Ltd. N^{ε}-(carbobenzoxy)-L-lysine, *N*-t-butoxycarbonyl-L-valine (Boc-L-Val) and triphosgene were purchased from GL Biochem Ltd. Trifluoroacetic acid (TFA) was procured from Aladdin Reagent Co., Ltd. The hydrobromic acid solution (33 wt% in acetic acid) was manufactured by Sigma-Aldrich. ε-Benzyloxy-carbonyl-L-lysine N-carboxyanhydride (ZLys NCA) was prepared according to Daly's method.[19] All of the other chemicals were analytical grade reagents and were used as received without further purification.

Synthesis of the Triblock Copolymer Pluronic-PLL

The synthesis of Pluronic-PLL triblock copolymers has been described elsewhere.[20] In this paper, we used valine instead of phenylalanine. Briefly, the following three steps are shown in Scheme 1: (1) the conversion of the –OH end group of Pluronic into $–NH_2$, i.e., to prepare Pluronic-NH_2, (2) the ring-opening polymerization of ZLys NCA in the presence of Pluronic-NH_2, which acts as a macroinitiator, and (3) the removal of the benzyloxycarbonyl (CBZ) protecting group of Pluronic-PZLL using 33% HBr/HOAc, The following is a typical procedure that was used for the second step. In an oven-dried flask, 6.3 g (0.05 mmol) of Pluronic-NH_2 and 4.59 g (15 mmol) of ZLys NCA were dissolved in dried CH_2Cl_2 (70 mL). The flask was pur ged with nitrogen three times and he solution was stirred at room temperature for 72 h. The product mixture was filtered and purified by precipitation in chilled diethyl ether. After the product was dried completely, a powdery product was obtained.

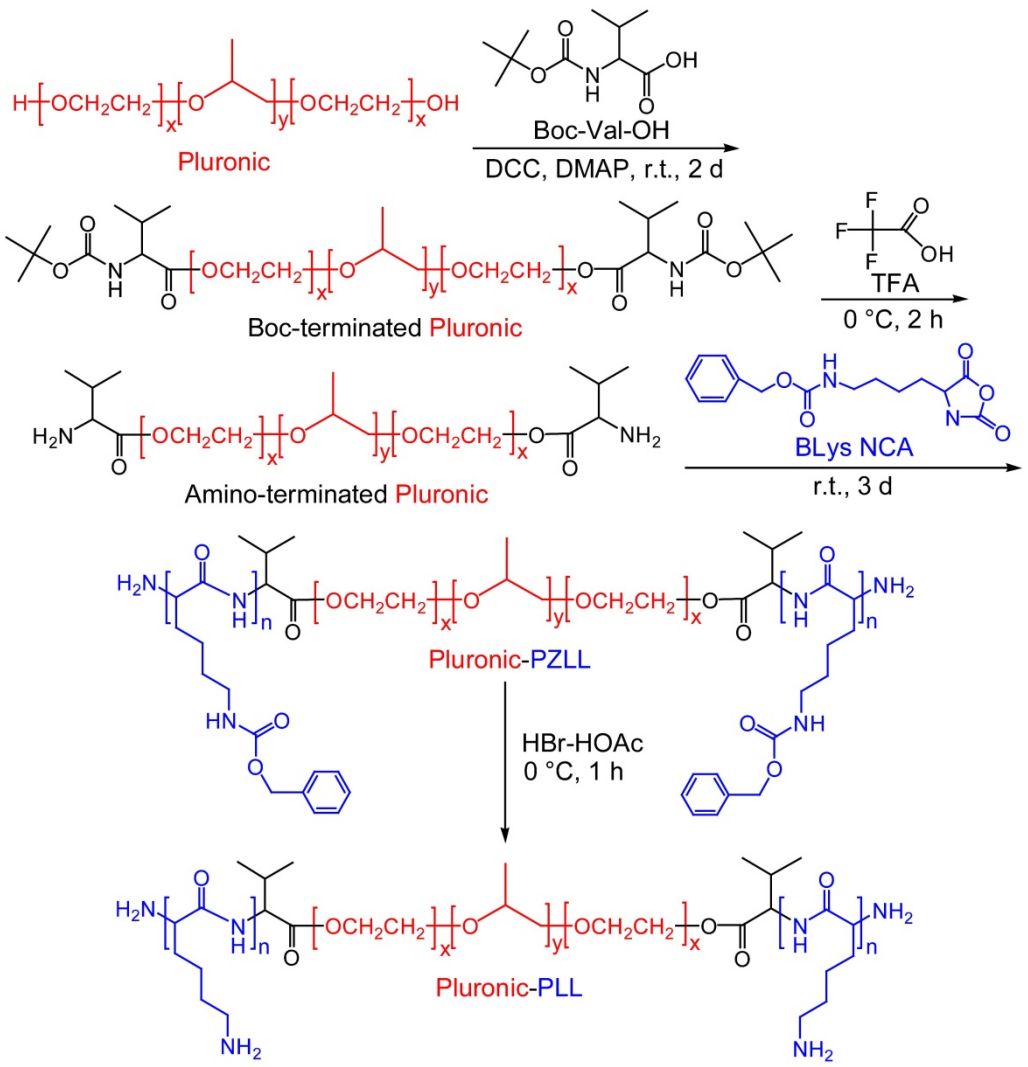

Scheme 1. Synthesis of the triblock copolymer Pluronic-PLL.

Sol-Gel Transition

The sol (flow)-gel (no flow) transition was determined by a test tube inversion method with temperature increments of 1 °C in each step.[21] Each sample with a given concentration was prepared by dissolving the polymer in distilled water in a 4-mL vial. After equilibration at 4 °C for 12 h, the vials containing the samples were immersed in a water bath at a constant designated temperature for 20 min. Inverting the vial determined whether a gel state was present using the criteria of no visually observed fluidity in 1 min. The sol-gel transition temperature determined by this method has a precision of ± 0.5 °C.

Micelle characterization

The CMCs of Pluronic-PLL were measured by the fluorescence spectroscopy method (Horiba, USA) using pyrene as a fluorescence probe. Pyrene was excited at 334 nm, and fluorescence spectra were recorded between 360 nm and 500 nm at polymer concentrations ranging from 5×10^{-3} to 10 mg/mL and a constant concentration of pyrene (6×10^{-7} mol/L). The measurement was carried out at 25 °C. The CMC values were estimated from the crossover point of the plots of the intensity ratio (I_{383}/ I_{372}) from pyrene excitation spectra *vs*. log C (where C is the concentration in mg/mL).

Synthesis of Cross-Linking Pluronic-PLL Nanoparticles with a Gold Nanoparticle Shell

A typical protocol was as follows: the gold nanoparticle shells on the cross-linking Pluronic-PLL nanoparticles were synthesized by adding 400 μL of $HAuCl_4$ (28 mmol) to a solution of Pluronic-PLL micelles with a final concentration of 2 mg/mL. Subsequently, the mixture was incubated for 1 h in a 37 °C water bath. Then, the Pluronic-PLL@Au nanoparticles were collected by centrifugation to remove free AuNPs.

Characterization

^{1}H NMR spectra were recorded on a Bruker Avance 400 NMR spectrometer, and the samples were dissolved in DMSO-d_6. The chemical shifts were given in ppm using tetramethylsilane (TMS) as an internal reference. UV-visible spectra were measured on a TU-1901 spectrophotometer using 1-cm path length quartz cuvettes. The spectra were collected within a range of 300 to 800 nm. The particle size distribution and zeta potential of the Pluronic-PLL and Pluronic-PLL@Au nanoparticles were determined using a MALVERN Zetasizer Nano ZS apparatus. Transmission electron microscopy (TEM, H-800 and JEM-2100F) was used to study the morphologies of the Pluronic-PLL@Au nanoparticles. Samples for TEM were prepared without centrifugation. The photothermal conversion performances of these Pluronic-PLL@Au nanoparticles aqueous dispersion (0.2 mL) at different concentrations (0.2-0.5 mg/mL) was irradiated by an 808-nm laser (Xi'an Laser Electronic Technology Co. Ltd. China), and the temperature of the dispersion was recorded once every 10 s by a thermocouple with an accuracy of ± 0.1 °C.

Fabrication of PTX-Loaded Pluronic-PLL@Au Nanoparticles

PTX was incorporated into Pluronic-PLL micelles by a solid dispersion method.[22, 23] Pluronic-PLL (30 mg, M_w = 29000) and PTX (400 μg) were added to 2 mL of methyl alcohol. After complete dissolution, the solvent was evaporated by rotary evaporation at 37 °C to obtain a solid PTX/ Pluronic-PLL matrix. Then, water was added to the matrix which was preheated in a warm water bath (60 °C), and the mixture was stirred for 30 min to obtain a micelle solution. After that, the PTX-loaded Pluronic-PLL micelles were filtered through a 0.22-μm filter. Finally, the PTX-loaded Pluronic-PLL@Au NPs were obtained by the addition of 100 μL of $HAuCl_4$ and incubation for 1 h in a 37 °C water bath. Free PTX were removed by centrifugation at 2000 rpm for 5 min. The PTX-loaded Pluronic-PLL@Au nanoparticles were collected by centrifugation at 8000 rpm to remove free AuNPs.

Drug release

The *in vitro* release properties of PTX from the Pluroinc-PLL@Au NPs were investigated by a dialysis method in an aqueous medium containing 1 mol/L sodium salicylate.[22, 24] The freeze-dried PTX-loaded Pluronic-PLL micelles and PTX-loaded Pluronic-PLL@Au nanoparticles were weighed, dissolved in 0.25 mL of water, and introduced into a dialysis membrane bag (MWCO = 7500 Da, Green Bird Science & Technology Development, Shanghai, China). The end-sealed dialysis bag was immersed into 25 mL of a 1 mol/L sodium salicylate solution at 37 °C. The experimental set-up was shaken horizontally at 75 rpm for 30 h. While the solubility of PTX in the release medium was 23 μg/mL, the maximum concentration of PTX in the medium was 1.8 μg/mL in this release experiment. Thus, sink conditions were assured. At predetermined time intervals, samples (0.5 mL) were withdrawn (0, 15, 30, and 45 min and 1, 2, 4, 6, 8, 10, 20, 24, and 30 h) and replaced with an equal volume of fresh medium. The samples were irradiated with an 808-nm NIR laser (1.0 W/cm^2) for 10 min at predetermined time intervals. The reverse-phase high-performance liquid chromatography (RP-HPLC) analysis of PTX in vitro was achieved on a C18 Gemini column (Phenomenex, California, USA) with a mobile phase consisting of acetonitrile/ammonium acetate buffer solution (10 mM, pH 5.0) (53:47, v/v) at a flow rate of 1.0 mL/min. The eluent was monitored by UV absorption at 227 nm. The determinations of the release of PTX from the stock solution and Taxol placed in a dialysis bag were conducted under the same conditions as the control. The encapsulation efficiency (EE) and loading efficiency (LE) of PTX were calculated as indicated below:

$$\text{EE (\%)} = (\text{Weight of PTX loaded}) / \text{Total amount of PTX} \times 100\%$$

$$\text{LE (\%)} = (\text{Weight of PTX loaded}) / \text{Weight of PTX-loaded nanoparticles} \times 100\%$$

Blood compatibility

Hemolysis test

Fresh whole blood containing sodium citrate was obtained from a healthy rabbit, and then it was diluted with saline water (1:1.25 V/V). Pluronic-PLL micelles and Pluronic-PLL@Au nanoparticles were dispersed in 1 mL of a 0.9% NaCl solution and incubated for 0.5 h at 37 °C in a water bath. Then, 20 μL of diluted whole blood was added into the materials solution and incubated for another 1 h. Positive and negative controls were produced by adding 20 μL of diluted blood to 1 mL of distilled water (hemolysis ratio is 0%) and saline water (hemolysis ratio is 100%), respectively. Afterwards, all samples were centrifuged at 2500 r/min for 10 min, and the supernatants were transferred to a 96-well plate. The optical density of the sample was measured at 450 nm using a microplate reader.[25] The hemolysis ratio was calculated according to the following equation:

$$\text{Hemolysis ratio} = \frac{\text{OD of test material-OD of negative control}}{\text{OD of positive control-OD of negative control}} \times 100\%$$

Plasma recalcification time

Platelet poor plasma (PPP) was obtained by centrifuging the whole blood (containing a 3.8 wt% citrate acid solution, blood/citrate acid = 9:1 V/V) extracted from a healthy rabbit at 3000 r/min for 10 min. Materials were dissolved in 1 mL of 0.025 mol/L $CaCl_2$ solution. One hundred microliter aliquots of the materials solution were placed into siliconized glass tubes, and positive and negative controls were also made by adding 100 μL of the 0.025 mol/L $CaCl_2$ solution to glass tubes and siliconized glass tubes, respectively. Then, all samples were incubated for 2 min in a 37 °C water bath, and at the end of that time period, 100 μL of PPP was dropped onto the samples. Timing began immediately, and the ending time was when the blood coagulated.

Dynamic clotting time

Materials were dissolved in 1 mL of 0.2 mol/L $CaCl_2$ solution. The concentrations of the materials in this experiment were the same as in the hemolysis test described above. The material solution was placed in siliconized glass tubes in 6.25 μL aliquots, and positive and negative controls were produced by adding 6.25 μL of 0.2 mol/L $CaCl_2$ solution to glass tubes and siliconized glass tubes, respectively. Then, 50 μL of whole rabbit blood was added onto the surface of the solution, and the solution was mixed uniformly. After 0 min, 2 min, 5 min, 10 min, 20 min, 40 min, 60 min, 100 min, and 160 min, the samples were diluted with 25 mL of distilled water and rinsed for a few minutes. The solutions were transferred to a 96-well plate, and the optical densities of the samples were determined at a wavelength of 540 nm using a microplate reader.[26] The relationship between the optical density and time was plotted as the clotting time curve, which indicates the relative clotting time of each sample.

Cell cultures

L02 cells and MDA-MB-231 breast cancer cells were cultured in DMEM containing 10% FBS, 100 U/mL penicillin, and 100 μg/mL streptomycin. All of the cells were grown at 37 °C in a CO_2 environment. The human monocytic leukemia cell line THP-1 was cultured in a RPMI-16 40 medium supplemented with 10% FBS, 2 mM L-glutamine, 1 mM Na-pyruvate, 5.0×10^{-5} M β-mercaptoethanol, 100 U/mL penicillin, and 100 μg/mL streptomycin.

In vitro cytotoxicity assays

Lactate Dehydrogenase Release Assay

L02 cells were obtained as a kind gift from the Key Laboratory of Drug Targeting and Novel Drug Delivery Systems (Sichuan University). The cells were seeded into 96-well plates, then treated with 100 μL of Pluronic-PLL and Pluronic-PLL@Au nanoparticle solutions (5 mg/mL). A 1% solution of Triton X-100 in DMEM and culture medium were used as a positive control and a negative control, respectively. After 72 h of incubation, the collected culture medium was centrifuged at 1500 rpm for 10 min.[27] Lactate dehydrogenase activity in the supernatant was determined using an LDH Cytotoxicity Assay Kit (Beyotime Biotechnology Co., Ltd.) according to the manufacturer's instructions.

Cytokine detection

The THP-1 cells (1.5×10^4 cells/well) were seeded in 96-well plates after stimulation with PMA. Differentiated cells were then stimulated with Pluronic-PLL and Pluronic-PLL@Au nanoparticle solutions (5 mg/mL) for 24 h. The levels of IL-1β and tumor necrosis factor alpha (TNFα) in the culture supernatants were determined using a commercial enzyme-linked immunosorbent assay (ELISA) kit (Senxiong Biotech Co., Ltd.) according to the manufacturer's instructions.[28]

MTT Assay

The cytotoxicity of the PTX-loaded Pluronic-PLL@Au NPs was evaluated using the MTT assay. MDA-MB-231 (1×10^4 cells/well) breast cancer cells were cultured in 96-well plates and incubated (37 °C, 5% CO_2) for 24 h in DMEM. Next, blank Pluronic-PLL@Au NPs, PTX-loaded Pluronic-PLL@Au NPs and Taxol with concentrations ranging from 0.02 to 20 μg/mL were added to the each well. After incubating for 24 h, 48 h and 72 h, 20 μL of the MTT solution (5 mg/mL, Sigma-Aldrich) was added to each well, and the samples were incubated for 4 h. Then, the medium was removed, and replaced with DMSO (150 mL), followed by 10 min of incubation. The absorbance was measured using a microplate reader (ELx800, Bio-Teks Inc.) at 490 nm.

Cell Viability Evaluation Using a Calcein-AM Assay

MDA-MB-231 cells (5×10^4 cells/well) were seeded into a cover glass-bottom dish and incubated (37 °C, 5% CO_2) for 24 h in DMEM. Then, 200 μL of the medium with blank Pluronic-PLL@Au NPs or PTX-loaded Pluronic-PLL@Au NPs (1 mg/mL) were added. After incubating for 24 h, the cells were irradiated with 1 W/cm^2 NIR light from the top for 10 min. The cells for chemotherapy alone were not exposed to NIR light. After irradiation treatment, cells were stained with 0.5 μM calcein-AM. The fluorescence images of MDA-MB-231 cells were observed using a fluorescence microscope (Olympus, Japan).

Cell Viability Evaluation Using an MTT Assay

MDA-MB-231 (1×10^4 cells/mL) breast cancer cells were cultured in 96-well plates and incubated (37 °C, 5% CO_2) for 24 h. Next, blank Pluronic-PLL@Au NPs, PTX-loaded Pluronic-PLL@Au NPs and Taxol with concentrations ranging from 0.02 to 20 μg/mL were added to each well. After incubating at 37 °C for 24 h, the cells were exposed to 808-nm 1 W/cm^2 NIR light for 10 min as the chemo-photothermal treatment. The cells for chemotherapy alone were not exposed to NIR light. After treatment, 20 μL of the MTT solution (5 mg/mL, Sigma-Aldrich) was added to each well, and the cells were further incubated for 4 h at 37 °C. Then, the medium was removed, and replaced with DMSO (150 mL) followed by 10 min of incubation. The absorbance was measured using a microplate reader (ELx800, Bio-Teks Inc.) at 490 nm.

Cell cycle

The MDA-MB-231 cells (1×10^5 cells/well) seeded into 6-well plates were incubated with Pluronic-PLL@Au NPs, Taxol, PTX-loaded Pluronic-PLL micelles or PTX-loaded Pluronic-PLL@Au NPs at an equivalent concentration of 0.6 μg/mL PTX for 24 h. Then, the cells were resuspended in ice-cold PBS at predetermined time points and fixed in 70% ethanol for 24 h at 4 °C. Subsequently, the cells were incubated with 0.1% RNase A for 1 h at 37 °C and stained with PI for 30 min in the dark. The DNA content was determined using FAC Scan flow cytometry. The cells that were not treated were used as the control.

Cellular uptake

Fluorescence microscopy

Rhodamine B (RB) was encapsulated in the NPs as a probe for the cellular uptake study. The RB-loaded Pluronic-PLL@Au nanoparticles were collected by centrifugation to remove free RB. The MDA-MB-231 cells (1×10^5 cells/well) seeded into 6-well plates were incubated with RB-loaded Pluronic-PLL@Au NPs and free RB at the designated RB concentration (20 μg/mL) for 24 h, 48 h and 72 h. The fluorescence images of MDA-MB-231 cells were observed using a fluorescence microscope (Olympus, Japan).

Confocal laser scanning microscopy

MDA-MB-231 cells were seeded in 6-well plates at a density of 8×10^4 cells/well and cultured for 24 h. A total of 500 mL of RB-loaded Pluronic-PLL@Au NPs and free RB at the designated RB concentration (20 μg/mL) were added. After incubation for 48 h, the cells were gently washed with PBS three times and then fixed with 4% formaldehyde for 30 min. Finally, the cells were incubated for an additional 10 min with DAPI and then washed with PBS three times. The cellular uptake experiments were performed on a confocal laser scanning microscope (CLSM, FV 1000, Olympus).

Tumor model

Each female Balb/c nude mouse (4-5 weeks, 18±2 g, Shanghai SLAC laboratory animal Co., Ltd.) were injected subcutaneously with 1×10^4 MDA-MB-231 cells into the flank region. The experiment was not carried out until the volume of the tumor grew to approximately 100 mm^3. All animal procedures were performed according to the research protocol approved by the Animal Care and Use Committee of Shanghai Cancer Institute.

Observation of the tumor frozen section

The free RB and RB-loaded Pluronic-PLL@Au NPs were administered via tail vein injection at an equivalent concentration. The isolated tumor tissues were put into a paraformaldehyde solution (4 mg/mL) and frozen rapidly to -70 °C for 2 h. The specimens were embedded in optimal cutting temperature (OCT) compound and cut into 5-mm histology slices by the cryostat. [29] Each section was picked up on a coverslip. Finally, the frozen sections were observed using a fluorescence microscope (Olympus, Japan).

In vivo distribution of Pluronic-PLL@Au NPs

DiR (1,1-dioctadecyl-3,3,3,3-tetramethylindotricarbocyanine iodide) was encapsulated in the NPs as a probe for the in vivo distribution study. Free DiR and DiR-loaded Pluronic-PLL@Au NPs were administered via tail vein injection at an equivalent concentration. At 2 h, 8 h and 48 h post-injection, the cancer-bearing mice were anesthetized with pentobarbital, and thefluorescence images were captured at the predetermined intervals using a Bruker In vivo Xtreme Fluorescence Imaging System.

In vivo chemo-photothermal therapy

The cancer-bearing mice were randomized into 5 treatment groups (n = 6 per group): PBS treatment (Group I), PTX treatment (6.5 μg per mouse, Group II), PTX-Loaded Pluronic-PLL micelles (Group III), Pluronic-PLL@Au NPs with laser treatment (Group IV), and PTX-loaded Pluronic-PLL@Au NPs with laser treatment (equivalent PTX dosage of 6.5 μg per mouse, Group V). The mice were administered treatments through tail veins. After 8 h of therapy, the tumors (Group IV and V) were locally irradiated by an 808-nm NIR laser at a laser power output of 1.0 W/cm^2 for 2 min. The temperature was recorded using an infrared camera thermographic system (IRS System, Inc., China). The sample solution was given

once every 3 days over a 30-day period. The weight and tumor volumes were measured once every 3 days. The tumor volume was calculated by the formula V = (tumor length×tumor width^2)/2. The tissue of the tumor, heart, liver, spleen, lung and kidney were examined with HE stain.

Statistical analysis

Microsoft Office Excel was used for statistical analysis. Data were presented as the mean ± standard deviation and analyzed by one-way analysis of variance (ANOVA) and Student's t-test. The statistical significance was set at $P < 0.05$.

Results and Discussion

Synthesis of the triblock copolymer Pluronic-PLL

We obtained Pluronic-PLL through the ring-opening polymerization (ROP) of NCA using amino-terminated Pluronic as a macromolecular initiator (Scheme 1).[30,31] The results are summarized in Table 1. Unless otherwise stated, the following experiments were performed using polymer P1. The formation of Pluronic-PLL was confirmed by the ^{1}H NMR spectrum, as shown in Fig. 1. Boc-L-Val end-capped Pluronic was obtained by the reaction of *N*-t-butoxycarbonyl-L-valine with Pluronic. Compared with the ^{1}H NMR spectrum of Pluronic in Figure 1A, the peak d in Figure 1B at 1.35 ppm is attributed to the $-CH_3$ of the protecting group. In Figure 1D, the peaks at 7.3 ppm (h, singlet, C_6H_5-), 5.0 ppm (g, -CH_2-), 2.97 ppm (f, -CH_2-), 1.73 ppm (e, -CH_2-) and 1.38 ppm (d, -CH_2-) were observed due to protons of the PZLL block. The peaks at 3.48 ppm (b, -CH_2-) and 1.04 ppm (a, -CH_3) were assigned to protons of the Pluronic block. The benzyloxycarbonyl group of the polymer can be removed in a HBr/acetic acid solution.[32] The deprotection was confirmed by ^{1}H NMR as shown in Fig. 1(E). In the ^{1}H NMR spectrum, the benzyl peaks at 7.3 ppm (h, singlet, C_6H_5-) and 5.0 ppm (g, -CH_2-) disappeared, indicating the completion of deprotection.

Sol-Gel Transition

The Pluronic-PLL block copolymer is quite hydrophilic, and thus, P1 is soluble in water. The concentrated polymeric aqueous solution could form a physical hydrogel with a *sol-gel* transition between room and body temperatures without the use of any chemical initiator (Figure 2A).

Pluronic F127 is an amphiphilic triblock copolymer with the formula PEO_{100} -PPO_{65}-PEO_{100}, in which PPO acts as the hydrophobic core and PEO acts as the corona. A distinctive feature of Pluronic copolymers is that they exhibit a sol-gel transition behavior in aqueous solution when the temperature is increased above their lower critical solution temperatures (LCSTs).[33, 34] Pluronic-PLL block copolymer has this property. The effect of PLL block length on the sol-gel transition curve is presented in Figure 2B. The curve shifted to higher concentrations by approximately 2.5 wt% and higher temperature with an increase of 3000 Da in the molecular weight of PLL, whereas the overall curve shape remained unchanged, i.e., with increasing hydrophilic block length, gelation takes place at a higher concentration and a higher temperature.

Critical micelle concentration (CMC)

The critical micelle concentration (CMC) is an important parameter that influences the in vitro and in vivo stability of micelles. Pluronic-PLL amphiphilic block copolymers can form spherical micelles through self-assembly. The CMC of Pluronic-PLL was determined using a fluorescence technique with pyrene as a hydrophobic probe. Figure 2C shows the ratio of I_{383}/I_{372} vs. the concentration of the copolymers plots.

Below a certain concentration, I_{383}/I_{372} is constant, and above this concentration, I_{383}/I_{372} increases with an increase in log C, eventually reaching a plateau. The CMC values of 1.74 mg/mL (Fig. 2C(a)), 2.22 mg/mL (Fig. 2C(b)) and 2.57 mg/mL (Fig. 2C(c)) were obtained from the crossover points of the plots.

Table 1. Feed composition and molecular characteristics of the triblock copolymer Pluronic-PLL

Polymer	Pluronic-NH_2:NCA (In feed)	M_n×10^{-4} (GPC)	M_w×10^{-4} (GPC)	M_w/M_n	CGC[a] (wt%)	CMC[b] (mg/mL)	Size[c] (nm)
P1	1:20	1.81	1.84	1.02	17 (42 °C)	1.74	82±1.9
P2	1:30	2.06	2.08	1.01	19.5 (44 °C)	2.22	87±1.1
P3	1:40	2.33	2.4	1.03	22 (44 °C)	2.57	91±2.1

[a] The critical gel concentrations (CGCs) were obtained from the phase diagram in Figure 2B.

[b] The critical micelle concentrations (CMCs) measured by a fluorescence technique using pyrene as a probe at 25 °C were obtained from Figure 2C.

[c] The average particle size diameter of the Pluronic-PLL micelles were determined using a MALVERN Zetasizer Nano ZS apparatus. The measurement was carried out at 20 °C and repeated 3 times.

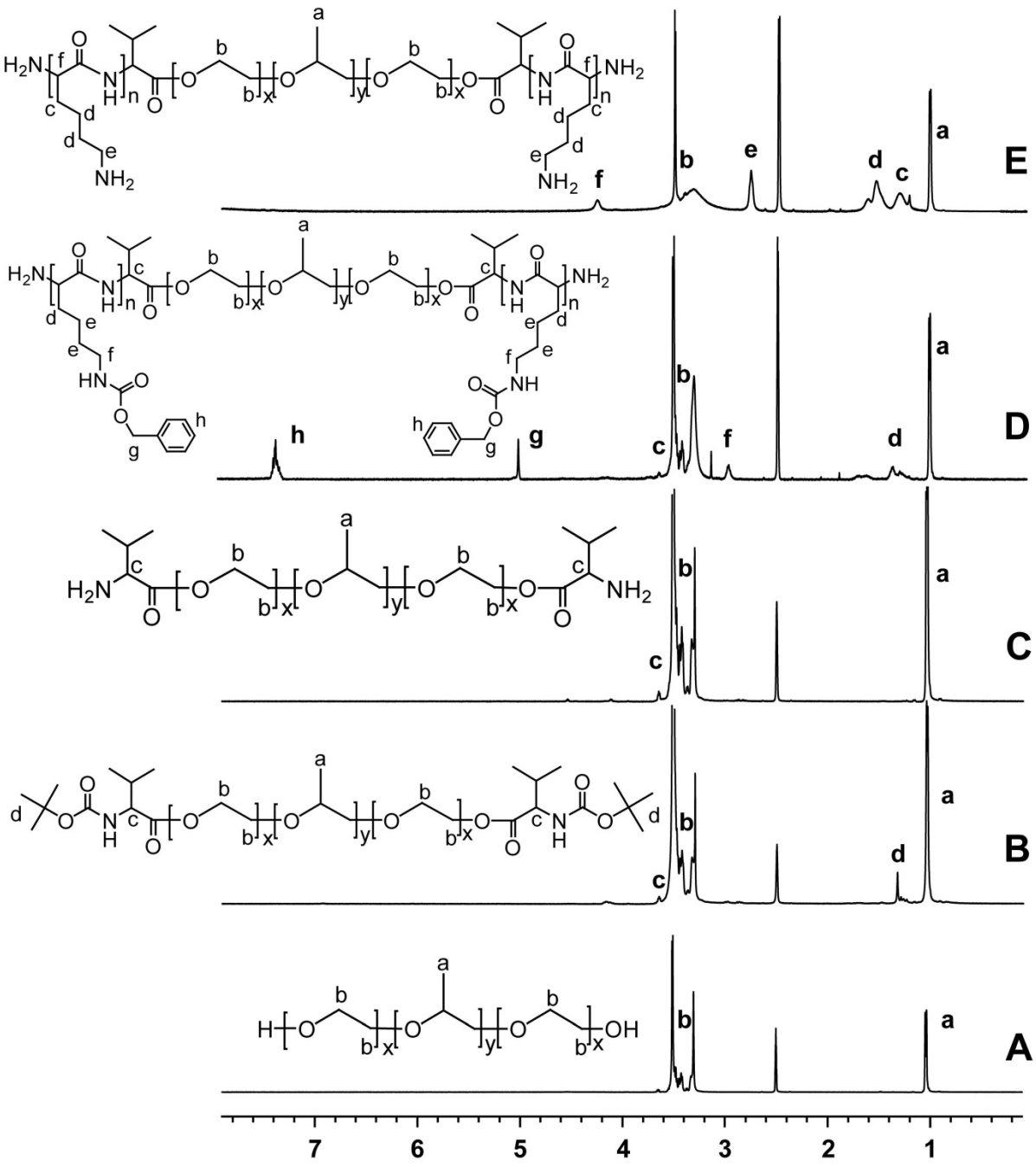

Figure 1. The ^{1}H NMR spectra and their assignments of (A) Pluronic, (B) Boc-L-Val end-capped Pluronic, (C) Pluronic-NH_2, (D) Pluronic-PZLL and (E) Pluronic-PLL in DMSO-d_6.

Synthesis of Micelles of Cross-Linking Pluronic-PLL Nanoparticles with Gold Nanoparticle Shells

Scheme 2 displays the synthesis route for Pluronic-PLL@Au NPs. Pluronic-PLL amphiphilic block copolymers can form micelles through self-assembly above the critical micelle concentration (CMC). The hydrophilic PLL block, which has abundant amino groups, is on the outside surface of the micelles.

Different weights of Pluronic-PLL were used to investigate its ability to reduce $HAuCl_4$ and stabilize the micelles formed with gold nanoparticle-coated Pluronic-PLL nanoparticles. When an aliquot of aqueous $HAuCl_4$ solution was added to aqueous solutions of Pluronic-PLL micelles at different micelle concentrations, a blue violet-colored solution was formed by standing for 1 h at 37 °C. As seen in Figure 3A, the solution color became darker with increasing micelle concentrations. However, the darker solution resulted in the agglomeration and precipitation of

nanoparticles within 2 days of standing at room temperature. When the concentration of Pluronic-PLL was increased, many more gold nanoparticles were adsorbed on the surface of the Pluronic-PLL micelles, which would easily lead to the precipitation of Pluronic-PLL@Au nanoparticles. This observation indicates that Pluronic-PLL is potent at reducing $HAuCl_4$. Transmission electron microscopy (TEM) images show that blank Pluronic-PLL micelles displayed a spherical shape with diameter of 50-70 nm (Figure 3B(a)) and that Pluronic-PLL forms rod-like micelles at a high concentration (3.5 mg/mL) (Figure 3B (c)). Gold nanoparticles were distributed on the surface of the rod-like micelles, and there were also a few free gold nanoparticles in the solution. Gold nanoparticles can improve the stability of micelles because the properties of the inorganic material are less affected by the solution concentration, temperature and pH. The as-synthesized Pluronic-PLL@Au nanorods have an average size of 150×50 nm. As seen in Figure 3B (b), spherical Pluronic-PLL@Au nanoparticles with diameters in the range of 60 to 80 nm were formed when the concentration of Pluronic-PLL was 2.5 mg/mL. After laser irradiation for 2 min, the morphology of Pluronic-PLL@Au nanoparticles remained unchanged (see Figure S1 in the Supporting Information). The chemical composition of the Pluronic-PLL@Au nanoparticles was investigated by EDS (see Figure S2 in the Supporting Information). The result shows the presence of C, O, and Au in the Pluronic-PLL@Au nanoparticles. We further measured the UV-vis spectra of mixed solutions of $HAuCl_4$ and Pluronic-PLL (2.5 mg/mL) at different reaction times (37 °C). As shown in Figure 3C, the UV-vis spectra of samples at different preparation stages were tested. The spectrum of Pluronic-PLL micelles did not show significant peaks in the range of 400 nm to 900 nm. The corresponding UV-vis spectra of Pluronic-PLL@Au NPs reflect the development of an SPR band ranging from 550 nm to 900 nm over time. The increased diameter of the AuNP could be the reason for the slight redshift of the SPR peak during the reaction from 0.5 h to 5.5 h. In this report, AuNPs were prepared with the reduction of $HAuCl_4$ by Pluronic-PLL, but the exact mechanism of the reduction is unclear. The $-NH_2$ groups in molecular PLL may also act as a reducing group in the formation of AuNPs. The electrostatic attraction of the amino group in the PLL and the metal salt ions (here $AuCl_4^-$) in the solution provides an effective driving force for the formation and stabilization of the AuNPs.[35] The negatively charged AuNPs are adsorbed on the surface of the Pluronic-PLL micelles by electrostatic interactions. Unless otherwise stated, the following experiments were performed using Pluronic-PLL@Au nanoparticles (1 h, 2.5 mg/mL of Pluronic-PLL).

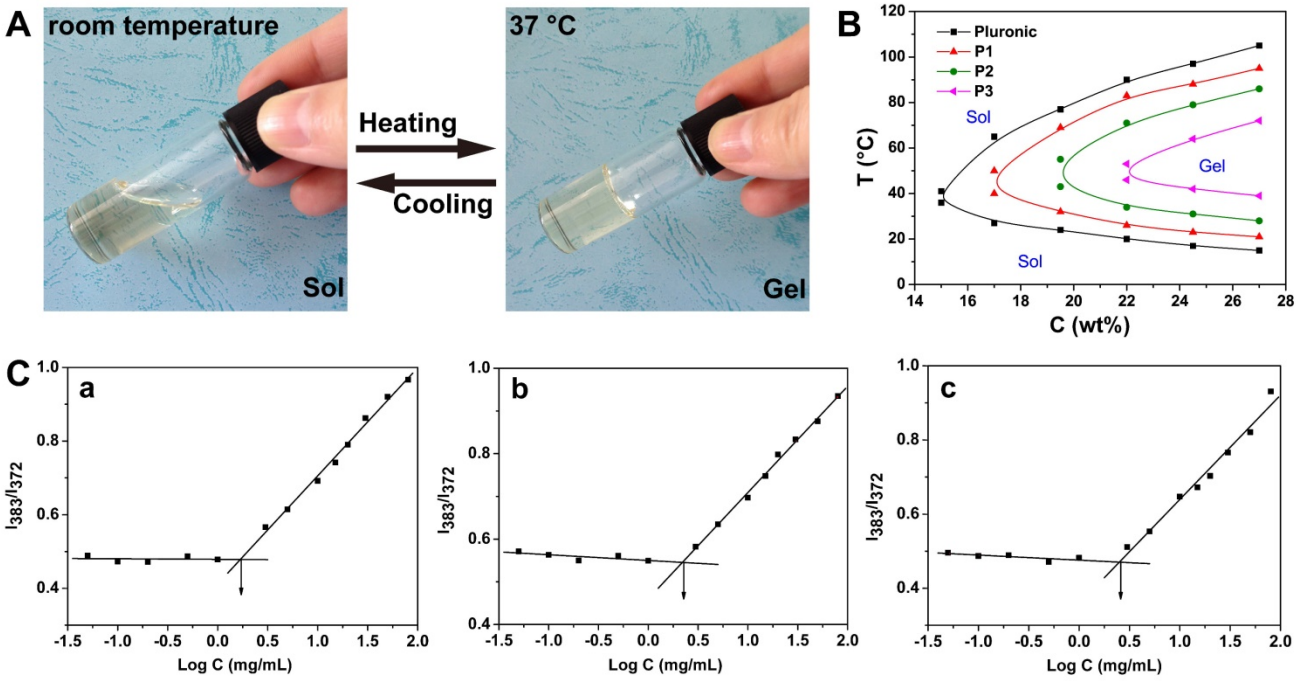

Figure 2. (A) Photographs of the P1 polymer solution (20 wt% in water) exhibiting a *sol* state at room temperature and a *gel* state after being heated to body temperature. (B) Phase diagrams of the Pluronic-PLL block copolymers Pluronic, P1, P2 and P3 in water at various temperatures (T) and concentrations (C). (C) Plots of I_{383}/I_{372} versus the logarithm of the concentration of the Pluronic-PLL block copolymers for (a) P1, (b) P2, and (c) P3. The I_{383}/I_{372} intensity ratio refers to the fluorescence emission of pyrene probe in experiments performed at 25 °C.

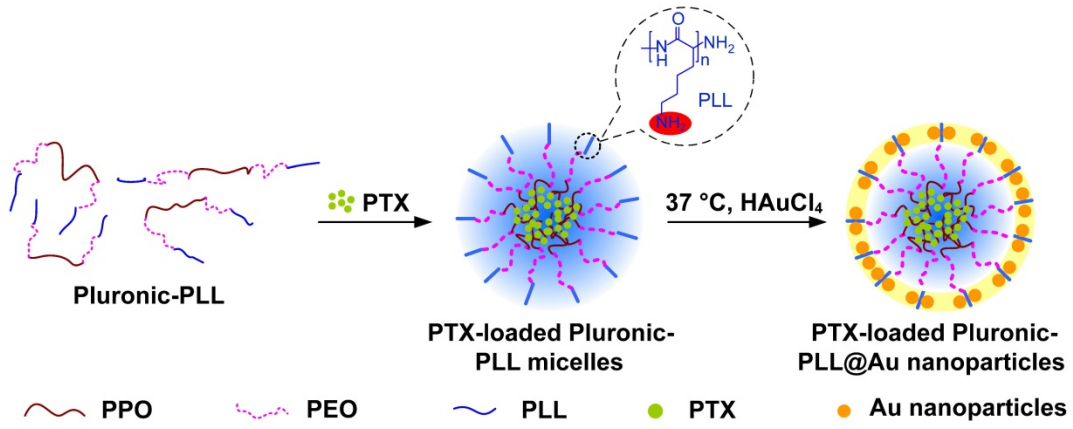

Scheme 2. Synthesis of PTX-loaded Pluronic-PLL@Au nanoparticles.

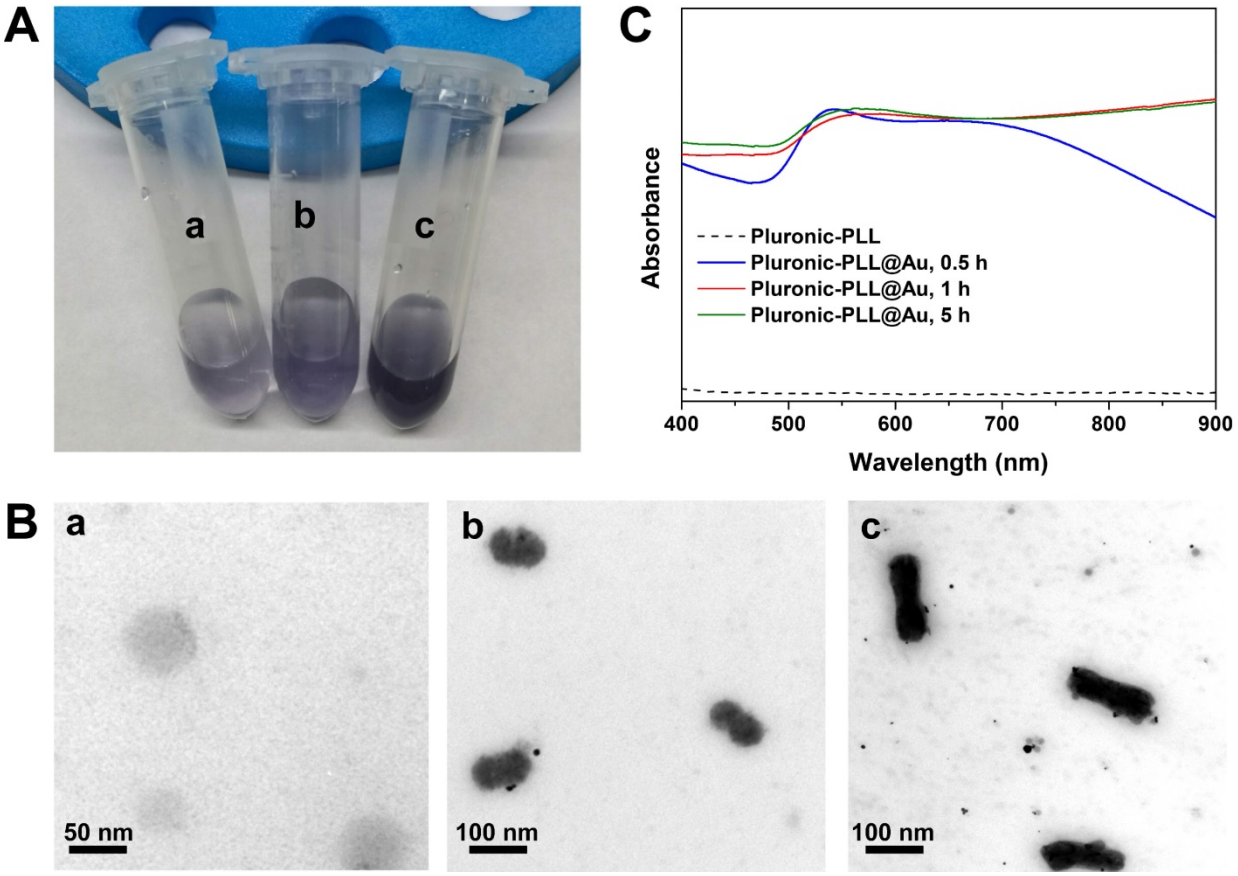

Figure 3. (A) Visual color of Pluronic-PLL@Au nanoparticles at different concentrations of Pluronic-PLL: (a) 2.5 mg/mL, (b) 3.5 mg/mL and (c) 5 mg/mL. (B) TEM images of Pluronic-PLL micelles (a) and Pluronic-PLL@Au nanoparticles at different concentrations of Pluronic-PLL: (b) 2.5 mg/mL and (c) 3.5 mg/mL. (C) UV-vis spectra obtained as a function of time after the addition of $HAuCl_4$ to the Pluronic-PLL solution at 37 °C.

It is well known that Pluronic micelles exhibit a thermo-sensitive assembly/disassembly behavior caused by thermally triggered hydrophobic interactions between the PPO segments.[36, 37] Figure 4A shows the sizes and zeta potentials of Pluronic-PLL@Au NPs (2.5 mg/mL of Pluronic-PLL) at different temperatures from 4 to 45 °C. The Pluronic-PLL@Au nanoparticles without or after laser irradiation both showed narrow size distributions, ranging from 70 to 100 nm with an average particle size diameter of 83 nm and 85 nm at 20 °C, respectively (see Figure S3 in the Supporting Information). Pluronic-PLL@Au NPs with a particle size distribution of 70-100 nm can be stored in PBS or 5% BSA for 3 days without significant agglomeration, indicating that the nanoparticles have shown good stability (see Figure S4 in the Supporting Information).

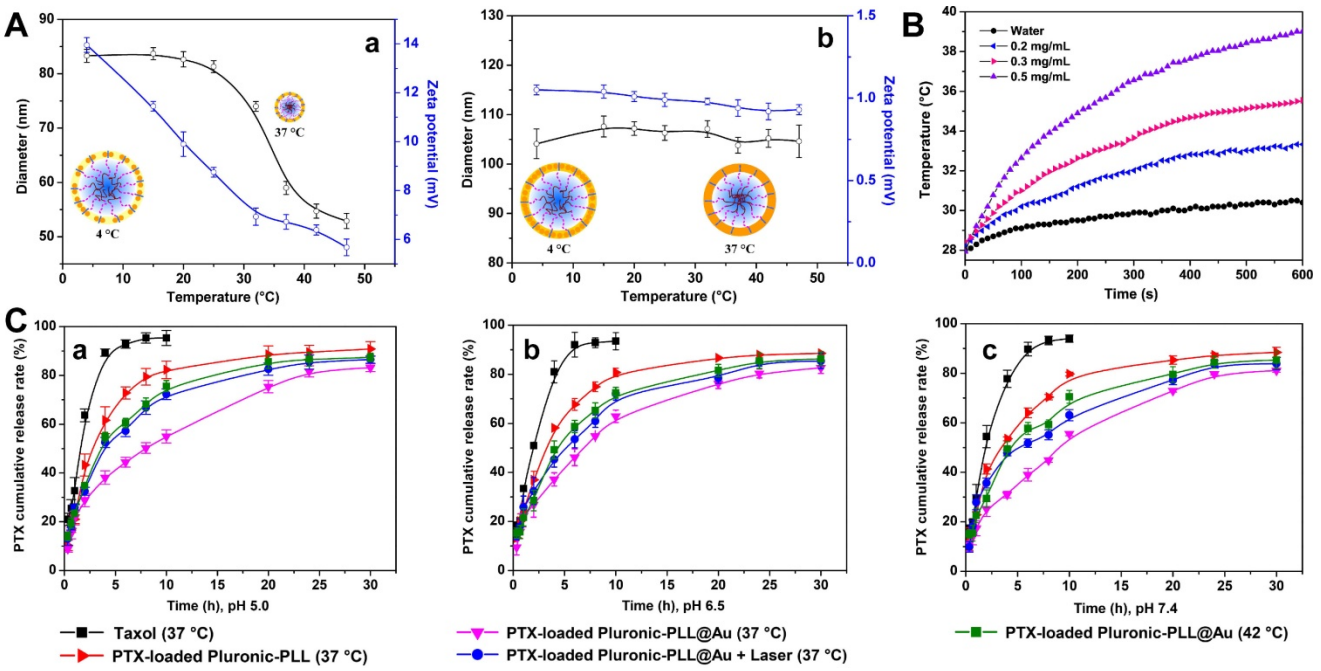

Figure 4. (A) Reversible swelling/shrinking behavior of Pluronic-PLL@Au nanoparticles prepared for different time periods: (a) 0.5 h and (b) 5.5 h. The data are presented as the mean ± S.D., n = 3. (B) Temperatures of Pluronic-PLL@Au nanoparticles at different concentrations under NIR laser irradiation (808 nm, 1 W) measured every 10 s with a digital thermometer over a period of 10 min. (C) Drug release profiles of PTX-loaded Pluronic-PLL micelles and PTX-loaded Pluronic-PLL@Au nanoparticles at 37 °C and 42 °C. The data are presented as the mean ± S.D., n = 3.

As seen in Table 1, the average particle size diameter of the Pluronic-PLL micelles increased with an increasing in the molecular weight of PLL. Hydrophilic segment growth increased the thickness of the hydration layer of Pluronic-PLL micelles. A broad thermal responsiveness over the temperature range is observed for the Pluronic-PLL@Au nanoparticles (Figure 4A(a), 0.5 h). Schematic illustrations of the Pluronic-PLL@Au NPs at 4 and 37 °C are also shown in the figure. The size of the Pluronic-PLL@Au NPs gradually shrank from 83 nm to 53 nm when the temperature of the solution rose from 4 to 45 °C. The shrinkage of the micelles will concomitantly decrease the average distance between gold nanoparticles and reduce the induced zeta potential. The shrinkage of Pluronic-PLL@Au NPs will induce a slight redshift of the SPR peak (see Figure S5 in the Supporting Information).

However, the size of the AuNPs prepared for 5.5 h is larger than that the AuNPs prepared for 0.5 h, as stated above. The average distance between the AuNPs is short. As seen in Figure 4A(b), the sizes and zeta potentials of the Pluronic-PLL@Au NPs had no significant changes when the temperature of the solution increased.

Photothermal Conversion Performance of the Pluronic-PLL@Au nanoparticles

AuNPs with near-infrared (NIR) light irradiation have been extensively employed in the photothermal treatment of solid tumors with the advantages of low cytotoxicity and excellent photostability.[38-40] To investigate the photothermal heating capabilities of Pluronic-PLL@Au NPs, Pluronic-PLL@Au NPs at different concentrations were exposed to an 808-nm NIR laser irradiation with a power density of 1 W. As shown in Figure 4B, the temperature of the pure water showed no significant changes in 10 min. The temperature of Pluronic-PLL@Au NPs aqueous dispersion at concentrations of 0.2, 0.3 and 0.5 mg/mL increased by 5.1, 7.5 and 11.1 °C, respectively, indicating that the 808-nm laser energy was efficiently converted into thermal energy.

Drug release

The PTX encapsulating efficiency of the Pluronic-PLL@Au NPs was 92.3 wt%, whereas the loading efficiency was 11.8 wt%. As we know, the pH of normal body tissue is 7.4, which is slightly alkaline, and tumors are more acidic than normal tissue. The release of PTX was studied under release mediums with pH values from 5.0 to 7.4 to mimic drug release in acidic tumor micro-environments and normal tissue. The in vitro cumulative release profiles of PTX from Pluronic-PLL micelles and Pluronic-PLL@Au NPs under simulated physiological conditions (PBS, pH = 7.4) and in an acidic environment (PBS, pH = 5.0 and 6.5) at different temperatures are shown in Figure 4C. The release of PTX from Taxol was also investigated as a control. The release rates were

apparently different under different conditions, which can be attributed to the different hydrophobic and ionic interactions between PTX and the Pluronic-PLL nanoparticles. The rate and amount of PTX released were not dependent on the pH of the medium. The in vitro release data showed that free PTX was released faster from the paclitaxel injection (Taxol) than from the Pluronic-PLL nanoparticles and that almost 100% of the PTX in the Paclitaxel injection was released after 10 h. The release behavior of PTX from the Pluronic-PLL nanoparticles exhibited almost the same release behavior, which consisted of an initial burst and a sustained release, as Pluronic-PLL@Au NPs at different temperatures. It can be concluded that the initial fast release is attributed to the drug being rapidly released from the outer region of the NPs, followed by sustained release from the core of the NPs.

The initial burst of PTX release was shown to last up to 2 h in Pluronic-PLL nanoparticles. After 30 h, the cumulative drug release approaches 90-96%. The results also showed that PTX was released more quickly from the PTX-loaded Pluronic-PLL nanoparticles than from the PTX-loaded Pluronic-PLL@Au NPs at 37 °C. The reason for this difference in the release of PTX can be attributed to the deposited Au nanoparticles on the surface of the Pluronic-PLL nanoparticles, which restricted the mobility of PTX and improved the stability of the Pluronic-PLL nanoparticles. Consequently, the release of PTX became slower. These results showed that PTX-loaded Pluronic-PLL nanoparticles had a more sustained release. For comparison, the PTX release profile of PTX-loaded Pluronic-PLL@Au NPs under the influence of the temperature of the medium was measured at 37 °C and 42 °C. As expected, the PTX release rate was enhanced at 42 °C. The particle size decreased with the increase in temperature, as can be seen in Figure 4A. The particle size at 42 °C is smaller than that at 37 °C; thus, more PTX was extruded at the higher temperature. The PTX release rate of the PTX-loaded Pluronic-PLL@Au NPs with laser irradiation was similar to that of the PTX-loaded Pluronic-PLL@Au NPs without laser irradiation when the medium was 42 °C.

Blood compatibility

A high plasma hemoglobin level is usually expressed as hemolysis and reflects the fragility of the erythrocyte membrane in contact with materials. The hemolysis ratios of Pluronic-PLL are shown in Table 2. The OD values for both the negative control and positive control are within the recommended values of ISO 10993-4.[41] As seen in Table 2, the hemolysis ratios of the P1, P2 and P3 micelles and Pluronic-PLL@Au NPs were less than 5% at a concentration of 2 mg/mL, which was came well within permissible limit.[42] The results indicated that these polymer materials can be used as biomaterials without causing hemolysis in the blood system.

Table 2. Hemolysis ratio (HR) and plasma recalcification time (PRT) of Pluronic-PLL micelles P1, P2 and P3 and Pluronic-PLL@Au NPs

Samples	HR (%)	PRT (s)
Negative control	/	249±4
Positive control	/	196±3
P1	3.45	314±4
P2	3.55	334±3
P3	4.01	321±6
Pluronic-PLL@Au	3.89	325±3

Table 2 also shows the PRT values of the Pluronic-PLL micelles and the Pluronic-PLL@Au NPs. The plasma recalcification time was measured to compare the substrate-induced delay in clotting or platelet-poor plasma following the activation of prothrombin in the presence of Ca^{2+}. The plasma recalcification times of the samples were 40% longer than that of the positive control. It can be concluded from this experiment that these polymer materials possess outstanding anticoagulant properties.

An in vitro dynamic blood clotting time test was conducted to evaluate the effect of the polymer materials on blood clotting time when they were in contact with blood. Figure 5A shows the dynamic clotting time curves of the Pluronic-PLL micelles and the Pluronic-PLL@Au NPs. The time at which the OD value equals 0.1 is generally defined as the initial clotting time. A longer clotting time indicates better clot resistance. It can be concluded that the OD values of the samples decreased with an increase in time and that the clotting times of the Pluronic-PLL micelles and Pluronic-PLL@Au NPs are longer than that of control, which indicated that the materials possessed outstanding anticoagulant properties.

In vitro cytotoxicity assays

Figure 5B demonstrates the cell viability after being cultured with Pluronic micelles, Pluronic-PLL micelles and Pluronic-PLL@Au nanoparticles for 24 h, 48 h and 72 h. Pluronic is commonly used in biomedical applications.[5,6] The cell viability of the MDA-MB-231 cells slightly decreases with an increase in the concentration of Pluronic micelles, Pluronic-PLL micelles and Pluronic-PLL@Au nanoparticles (to 80 % viability). Incubation time does not affect cell viability. Compared with Pluronic, there were no significant cytotoxic effects detected with the blank Pluronic-PLL micelles and the Pluronic-PLL@Au nanoparticles. The cell viability of

mouse fibroblast L-929 cells against Pluronic-PLL@Au nanoparticles after being cultured for 24 h and 48 h were above 85 %, also indicating that the Pluronic-PLL@Au nanoparticles had no cytotoxicity (see Figure S6 in the Supporting Information). Due to these results, it is believed that Pluronic-PLL micelles and Pluronic-PLL@Au nanoparticles have the potential to be good carriers for the delivery of anticancer drugs.

To further evaluate the cellular toxicity of Pluronic-PLL and Pluronic-PLL@Au, an LDH release assay was used to monitor plasma membrane damage. The LDH release levels in L02 cells at 24 h is shown in Figure 5C. The LDH concentrations of the negative control group and positive control group were 38.04 pg/mL and 105.81 pg/mL, respectively. The LDH concentrations of the P1, P2, P3 and Pluronic-PLL@Au groups were similar to that of the negative control (38.04 pg/mL) ($P > 0.05$), indicating that the LDH released in these samples was much lower than that in the positive control. This result confirmed the data obtained in the MTT assay, indicating that Pluronic-PLL and Pluronic-PLL@Au exhibited negligible toxicities.

Interleukin-1β (IL-1β) and tumor necrosis factor-α (TNF-a) play an important role in mediating inflammatory responses in fibrous and bony tissues. Therefore, we carried out systematic studies to determine the association between IL-1β and TNF-α. To assess the cytokine secretion of THP-1 cells in the culture medium of the samples, we employed an ELISA assay. We included 6.4% phenol as a positive control. The extracellular contents of IL-1β and TNF-α in THP-1 cells at 24 h are shown in Figures 5D(a) and 5D(b). The amounts of IL-1β released were 6.56 pg/mL, 5.28 pg/mL, 6.19 pg/mL and 8.6 pg/mL for the P1, P2, P3 and Pluronic-PLL@Au groups, respectively, which were similar to that of the negative control (9.2 pg/mL) ($P > 0.05$). The release amounts of TNF-α were 5.02 pg/mL, 4.63 pg/mL, 6.05 pg/mL and 6.19 pg/mL for the P1, P2, P3 and Pluronic-PLL@Au groups, respectively, which were also similar to that of the negative control (6.27 pg/mL) ($P > 0.05$). Thus, the Pluronic-PLL and Pluronic-PLL@Au nanoparticles caused significantly lower amounts of cytokine production compared with the positive control ($P < 0.05$), which might due to an inhibitory effect of the extracts on leukocyte activation. These findings indicate that Pluronic-PLL@Au nanoparticles have excellent biocompatibility.

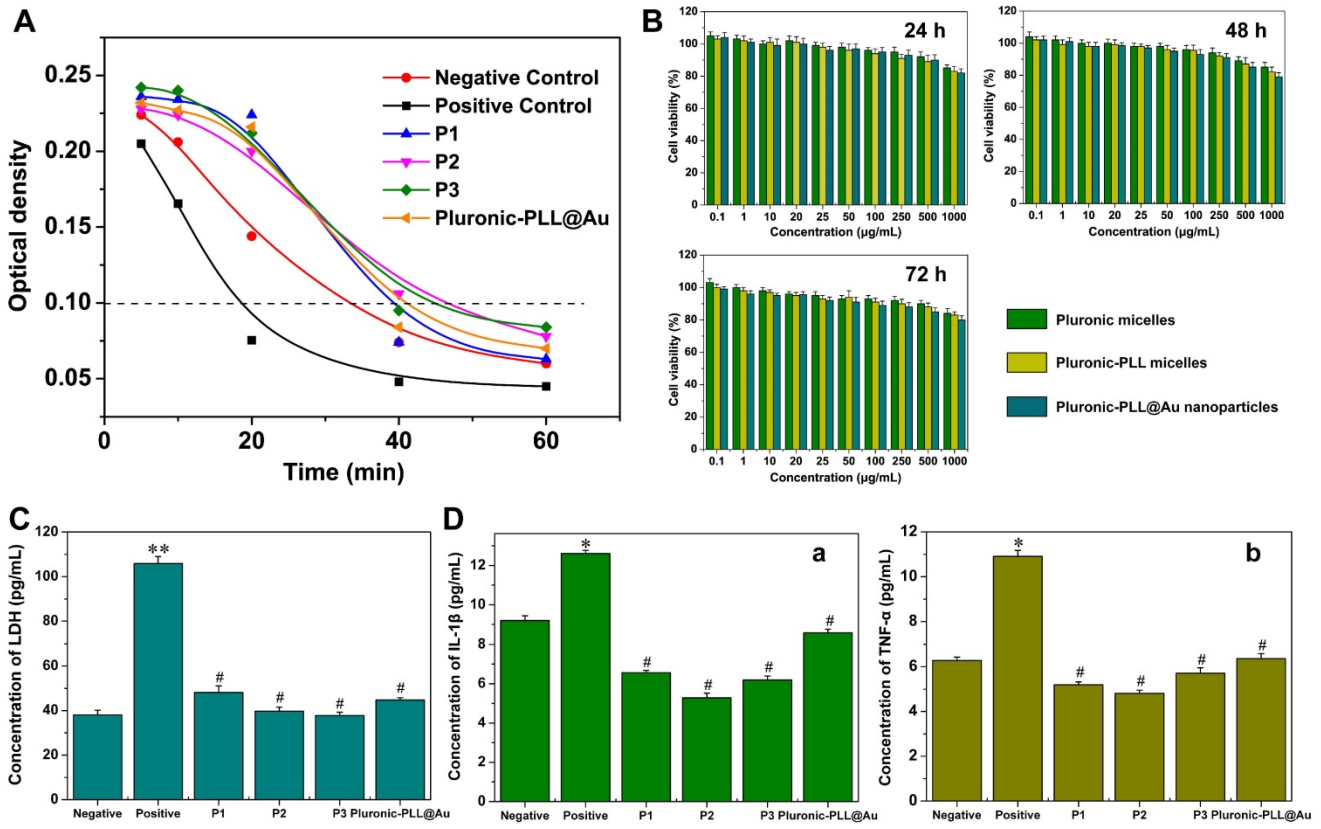

Figure 5. (A) Dynamic clotting time curves of Pluronic-PLL micelles P1, P2, P3 and Pluronic-PLL@Au NPs. (B) Cell viability of MDA-MB-231 cells against blank Pluronic, Pluronic-PLL (P3) micelles and Pluronic-PLL@Au nanoparticles after being cultured for 24 h, 48 h and 72 h at different concentrations. Data are presented as the mean ± S.D., n = 3. (C) Extracellular content of LDH in L02 cells. The data are presented as the mean ± S.D., n = 3. (D) Extracellular content of (A) IL-1β and (B) TNF-α in the THP-1 cell line. The data are presented as the mean ± S.D., n = 3; *p < 0.05, **p < 0.005, #p > 0.05 versus negative.

To evaluate the chemo-photothermal treatment, MDA-MB-231 cells incubated with PTX-loaded Pluronic-PLL@Au NPs were treated with and without NIR irradiation, and stained with calcein-AM green fluorescent dye, which is only incorporated into live cells.[43] Figure 6A (a) shows a fluorescence microscopy image of MDA-MB-231 cells incubated with Pluronic-PLL@Au nanoparticles. Most of the cells were alive, indicating that Pluronic-PLL@Au nanoparticles exhibited negligible toxicity. Figures 6A (b) and (c) show the fluorescence microscopy images of MDA-MB-231 cells incubated with Taxol (2.4 μg/mL) and PTX-loaded Pluronic-PLL@Au NPs (0.2 mg/mL, concentration of PTX is 2.4 μg/mL) for 1 d, respectively. The cells appeared to be alive in Figure 6A (b), more so than in Figure 6A (c). This result suggested that PTX-loaded nanoparticles exhibited a higher inhibition of MDA-MB-231 cells compared with Taxol. As shown in Figure 6A (d), after irradiating with an NIR laser for 10 min, few of the PTX-loaded Pluronic-PLL@Au NP-incubated MDA-MB-231 cells were alive compared with the result obtained from Figure 6A (c), indicating that the combination of PTX and photothermal treatment is better than chemotherapy treatment alone.

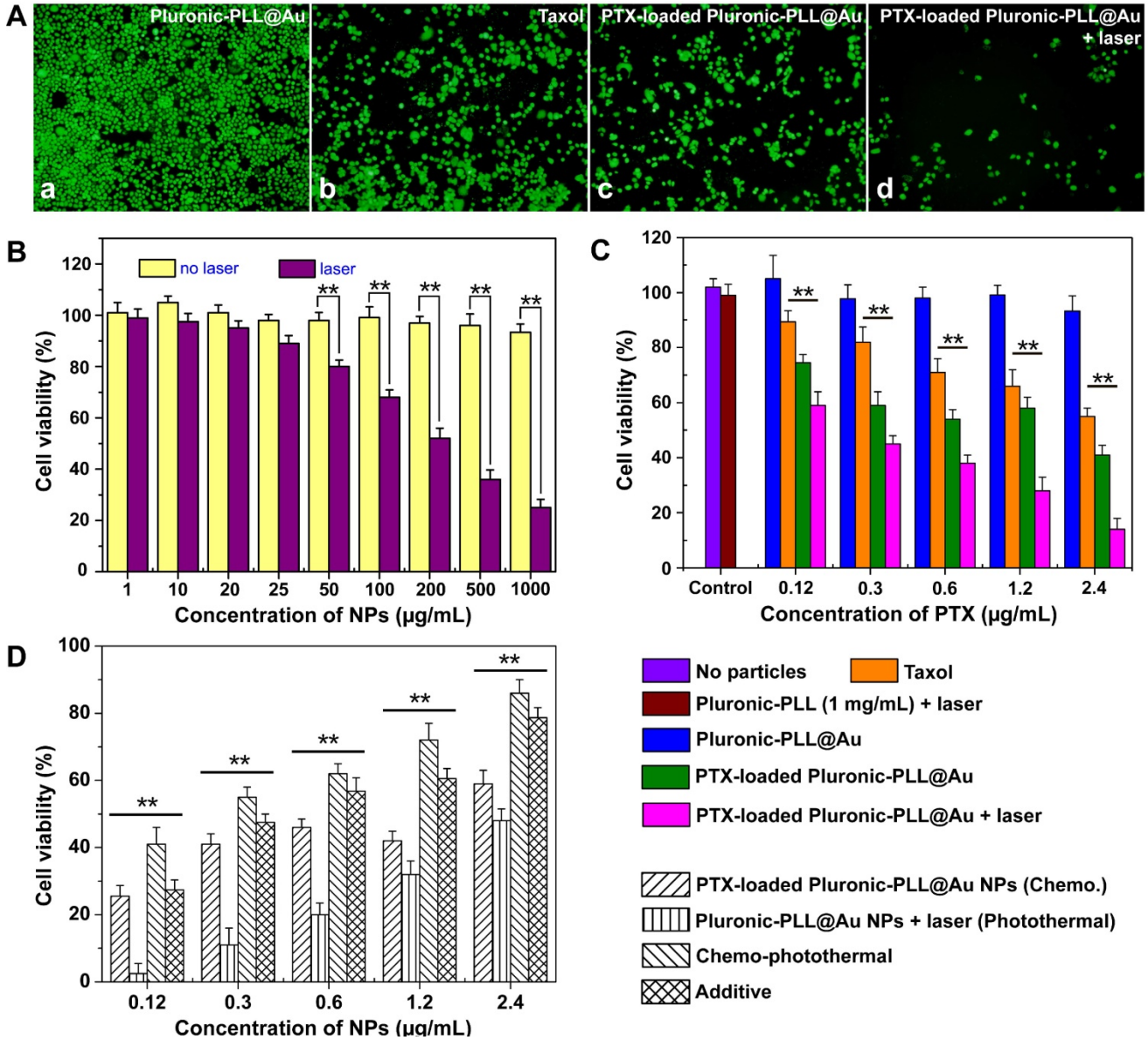

Figure 6. (A) Fluorescence microscopy images of MDA-MB-231 cells treated with Pluronic-PLL@Au nanoparticles, Taxol, PTX-loaded Pluronic-PLL@Au nanoparticles and PTX-loaded Pluronic-PLL@Au nanoparticles with 1 W/cm² NIR irradiation for 10 min. (B) After being incubated for 24 h, MDA-MB-231 cell viabilities at different dosages of Pluronic-PLL@Au nanoparticles (0.001, 0.01, 0.025, 0.05, 0.1, 0.25, 0.5 and 1 mg/mL) with or without laser irradiation (808 nm, 1 W/cm², 10 min). (C) Comparison of cell viability of MDA-MB-231 cells incubated with blank Pluronic-PLL@Au nanoparticles, Taxol and PTX-loaded Pluronic-PLL@Au nanoparticles with or without laser irradiation (808 nm, 1 W/cm², 10 min). (D) Therapeutic efficacy versus NPs concentration for different treatments. Data are shown as the mean ± SD, n = 3; **p < 0.005.

To further investigate the photothermal cytotoxicity of Pluronic-PLL@Au NPs *in vitro*, the Pluronic-PLL@Au NP-incubated MDA-MB-231 cells were treated with and without an NIR laser. Then, cell viability assays (MTT) were performed to investigate the cytotoxicity. As can be seen in Figure 6B, the cell viabilities of MDA-MB-231 cells without NIR irradiation were more than 90% at concentrations ranging from 0.001 to 1 mg/mL, suggesting that Pluronic-PLL@Au nanoparticles showed negligible cytotoxicity, even at higher concentrations. When the Pluronic-PLL@Au NP-incubated MDA-MB-231 cells were irradiated with an NIR laser for10 min, the cell viabilities decreased with an increase in concentration. At lower concentrations (1-25 μg/mL), no influence of laser irradiation was found on the Pluronic-PLL@Au NP-incubated cells. Under NIR irradiation, when the MDA-MB-231 cells were incubated with Pluronic-PLL@Au nanoparticles with a concentration over 0.5 mg/mL, about 70% of the MDA-MB-231 cells lost their viability. These results clearly indicated the significant photothermal therapeutic effect of a combination of Pluronic-PLL@Au NPs and NIR laser illumination.

For combined chemo and photothermal treatments, the PTX-loaded Pluronic-PLL@Au NP-incubated MDA-MB-231 cells were treated with and without NIR irradiation. Subsequently, we measured their viabilities using MTT (Figure 6C). A no nanoparticle group and a group of 1 mg/mL Pluronic-PLL micelles with laser irradiation were used as controls. The PTX concentration at each point was 0.12, 0.3, 0.6, 1.2 and 2.4 μg/mL, where 0.12, 0.3, 0.6, 1.2 and 2.4 μg/mL PTX were estimated to be contained in 10, 25, 50, 100 and 200 μg/mL Pluronic-PLL@Au NPs, respectively. Figure 6C showed that Pluronic-PLL micelles with laser irradiation had no effect on cell survival. Both free PTX and PTX-loaded Pluronic-PLL@Au NPs showed dose-dependent cytotoxicity. The PTX-loaded NPs showed higher cytotoxicity than Taxol at equivalent PTX concentrations ($P < 0.005$), indicating that PTX-loaded Pluronic-PLL@Au NPs exhibit higher inhibition of the proliferation of MDA-MB-231 cells after a 24-h culture. PTX-loaded Pluronic-PLL@Au NPs with laser irradiation exhibited lower cell viability than treatment with PTX-loaded Pluronic-PLL@Au NPs alone ($P < 0.005$). The above results reveal good agreement with the calcein-AM assay. Figure 6D shows the therapeutic efficacy of different treatments at various concentration of NPs. The therapeutic efficacies were calculated by subtracting the cell viability from 100%. The additive therapeutic efficacies were estimated using the formula of $T_{additive} = 100 - (f_{chemo} \times f_{photothermal}) \times 100$.[15] The results showed that chemo-photothermal co-therapy caused a synergistic effect; thus, the co-therapeutic efficacies were higher than the additive therapeutic efficacy of chemo- and photothermal therapy.

Cell cycle

The cell cycle distribution of the MDA-MB-231 cells incubated with Pluronic-PLL@Au NPs, Taxol, PTX-loaded Pluronic-PLL micelles or PTX-loaded Pluronic-PLL@Au NPs with laser irradiation is shown in Figure 7. Compared with cells treated with Pluronic-PLL@Au NPs, the number of cells treated with Taxol or PTX-loaded Pluronic-PLL micelles decreased in the G0/G1 phase and S phase and increased in the G2/M phase, which indicated cell arrest in the G2/M phase. It is well known that PTX inhibits cell cycle progression in the G2/M phase, which demonstrated that the DNA was damaged and repaired in cells. However, the analysis also showed that PTX-loaded Pluronic-PLL@Au NPs with laser irradiation cause an arrest in the S-to-G2/M phase transition with a significant decrease in the amount of cells in the G0/G1 phase and a significant increase in the S phase and G2/M phase. The present results suggested that the inhibition mechanism of PTX-loaded Pluronic-PLL@Au NPs with laser irradiation was different from that of PTX-loaded Pluronic-PLL micelles. The principle of photothermal therapy was used to convert the light energy into heat. Heat caused the denaturation of proteins and DNA. The detailed mechanisms will be investigated further.

Cellular uptake

The cellular uptake of RB-loaded Pluronic-PLL@Au nanoparticles by MDA-MB-231 cells was studied by fluorescence microscopy and compared with free RB cultured for 24 h, 48 h and 72 h to understand the effect of nanoparticles on cellular uptake. Because PTX itself is not fluorescent, RB was used as a marker instead of PTX. The concentration of RB was 20 μg/mL. As shown in Figure 8A, for MDA-MB-231 cells incubated for the same amount of time with an equivalent RB concentration in each formulation, the Pluronic-PLL@Au nanoparticles showed higher fluorescence intensities than free RB. For MDA-MB-231 cells incubated with free RB, the fluorescence intensity at 48 h was higher than those at 24 h and 72 h. This result illustrated that the cellular uptake of RB can be enhanced by Pluronic-PLL@Au nanoparticle loading. Additionally, the nanoparticles can extend the residence time of RB (drug) in MDA-MB-231 cells.

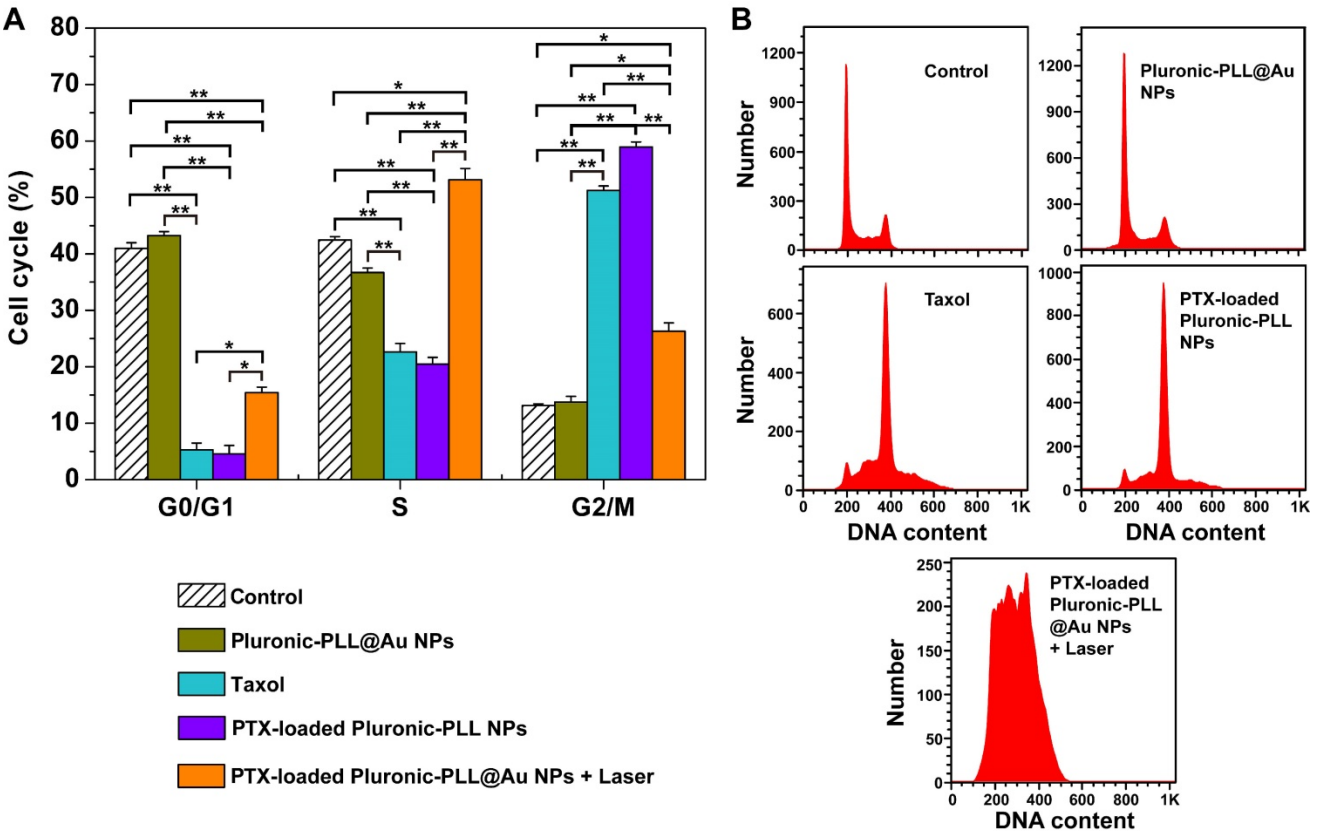

Figure 7. Flow cytometer analysis of cell cycle distribution of MDA-MB-231 cells incubated 24 h with Pluronic-PLL@Au NPs, Taxol, PTX-loaded Pluronic-PLL micelles or PTX-loaded Pluronic-PLL@Au NPs with laser irradiation at an equivalent concentration of 0.6 μg/mL PTX. Data are presented as the mean ± S.D. (n = 3). *p < 0.01, **p < 0.001.

CLSM was used to verify the effect of cellular uptake of the Pluronic-PLL@Au nanoparticles. RB was used as a marker instead of PTX. The nuclei of cells were stained with DAPI. MDA-MB-231 cells were incubated with RB-loaded Pluronic-PLL@Au NPs and free RB for 48 h and observed using CLSM. As shown in Figure 8B, the RB fluorescence intensity found in RB-loaded Pluronic-PLL@Au NP-incubated MDA-MB-231 cells is much higher than that of free RB-incubated cells, indicating that Pluronic-PLL@Au nanoparticles enhanced the cellular uptake efficiency in MDA-MB-231 cells. These results can be explained by two key factors. First, the zeta potential of Pluronic-PLL@Au nanoparticles used for the in vitro experiment was 6.72±0.3 mV (as shown in Figure 4A(a), 37 °C), which promoted NP adsorption onto negatively charged cell membranes.[44] Second, the diffusion of the free small drug molecule PTX (or RB marker) depends on the concentration gradient.[45] However, the cellular uptake of PTX (or the RB marker)-loaded NPs is unidirectional. Thus, the persistent intracellular release of PTX (or the RB marker) from the NPs might enhance the inhibition of MDA-MB-231 cell growth.

Tumor targeting of the NPs

We also investigated the drug distribution in tumor tissue treated with RB and RB-loaded Pluronic-PLL@Au NPs. Figure 8C shows the fluorescence microscopy images of a frozen section in MDA-MB-231 breast carcinoma-bearing mice at 48 h after the intravenous injection of free RB and RB-loaded Pluronic-PLL@Au NPs. As shown in Figure 8C, the tumor tissue treated with RB-loaded Pluronic-PLL@Au NPs exhibited significantly higher fluorescence signals than free RB. The ideal particle sizes (less than 200 nm) and enhanced permeability of the tumor are conducive to improving the targeted delivery efficiency of Pluronic-PLL@Au NPs.

In vivo distribution of Pluronic-PLL@Au NPs

Subsequently, the time-dependent biodistributions of DiR-loaded Pluronic-PLL@Au NPs and DiR-loaded Pluronic-PLL micelles were observed using a fluorescence imaging system after intravenous injections into MDA-MB-231 tumor-bearing mice. The fluorescence imaging is presented in Figure 9. DiR was used as a fluorescent dye. It is clear that the strongest tumor fluorescence signals were at 8 h for mice injected with free DiR or DiR-loaded

Pluronic-PLL@Au NPs. Therefore, laser irradiation was carried out 8 h after intravenous injections in vivo in chemo-photothermal therapy. At the 8 h point of injection, the tumor fluorescence signal of mice treated with DiR-loaded Pluronic-PLL@Au NPs was higher than that of mice treated with free DiR. As shown in Figure 9A, free DiR was eliminated in the tumor area 48 h post-injection. The tumor fluorescent signal of mice treated with DiR-loaded Pluronic-PLL@Au NPs can be maintained for at least 48 hours. The results were further quantitatively confirmed by the fluorescence signal data of the tumor (Figure 9B), indicating that the DiR-loaded Pluronic-PLL@Au NPs observably improve tumor targeting delivery efficiency *in vivo*.

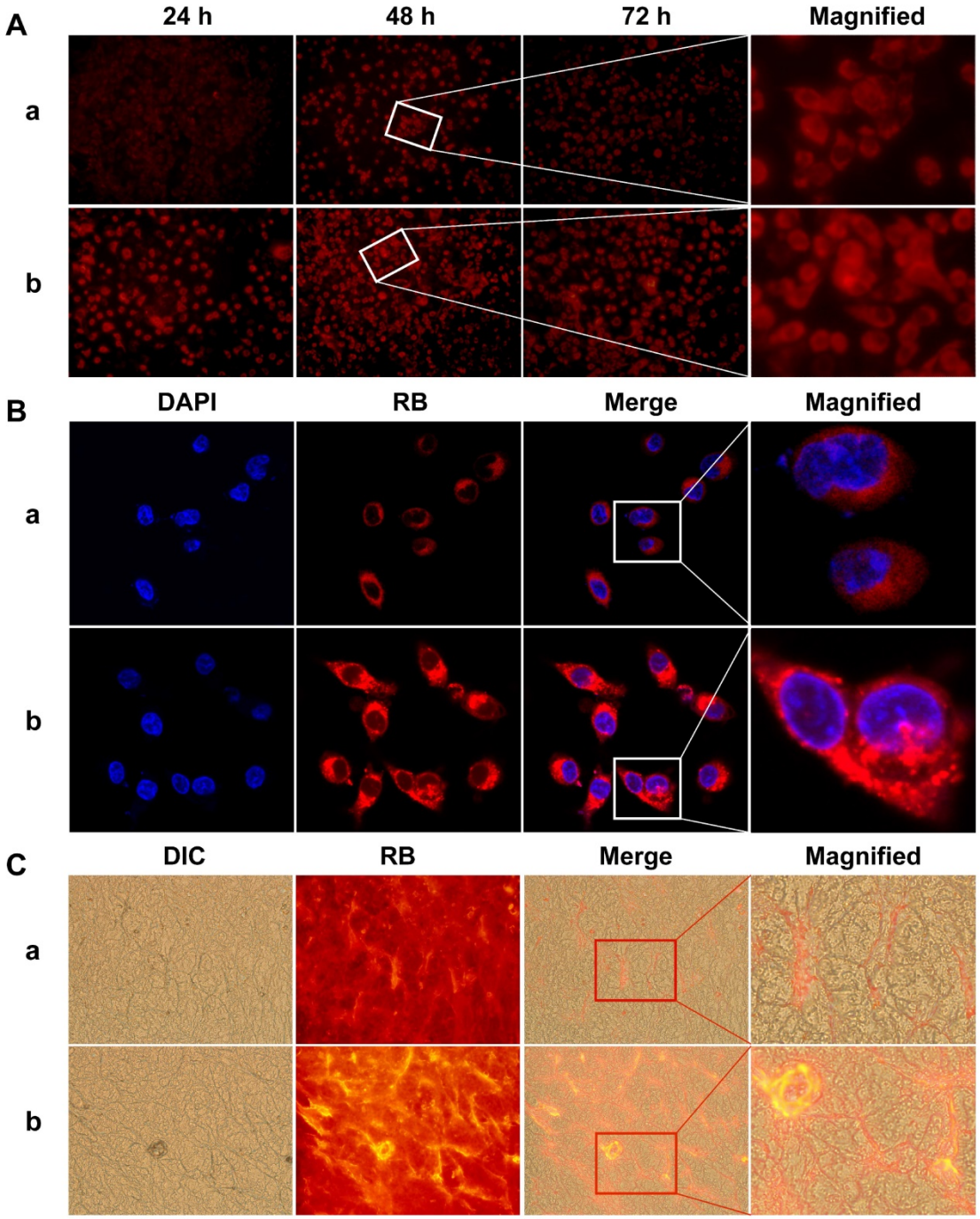

Figure 8. (A) Fluorescence microscopy images of MDA-MB-231 cells cultured with free RB (a) and RB-loaded Pluronic-PLL@Au nanoparticles (b, the concentration of RB was 20 μg/mL) for 24 h, 48 h and 72 h. (B) Confocal laser scanning microscopy (CLSM) images of MDA-MB-231 cells cultured with free RB (a) and RB-loaded Pluronic-PLL@Au nanoparticles (b, the concentration of RB was 20 μg/mL) for 48 h. (C) In vivo drug distribution in a tumor determined by fluorescence microscopy in MDA-MB-231 breast carcinoma-bearing mice at 48 h after the intravenous injection of free RB (a) and RB-loaded Pluronic-PLL@Au nanoparticles (b).

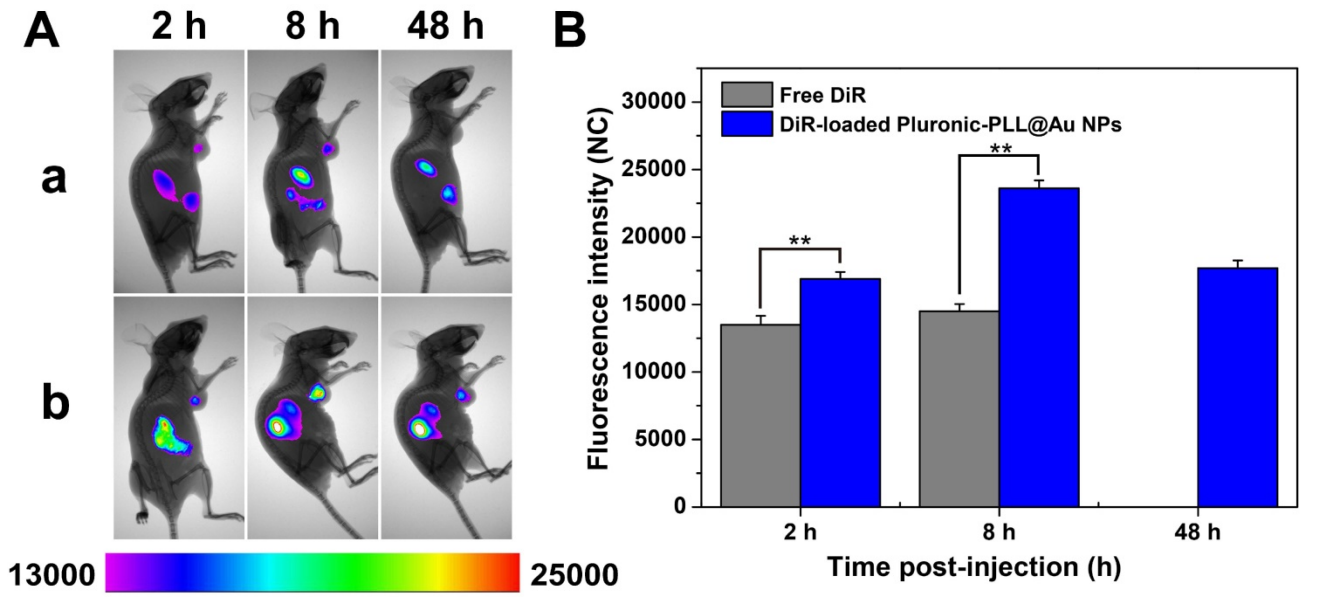

Figure 9. (A) In vivo time-dependent fluorescence image in tumor-bearing mice at 2, 8, 24 and 48 h after intravenous injection of free DiR (a) and DiR-loaded Pluronic-PLL@Au NPs (b). (B) The quantification of the tumor target characteristics of free DiR and DiR-loaded Pluronic-PLL@Au NPs. Data are presented as the mean ± S.D. (n = 3). **p < 0.001.

In vivo chemo-photothermal therapy

To evaluate the in vivo chemo-photothermal therapeutic effect of PTX-loaded Pluronic-PLL@Au NPs under irradiation, PTX-loaded Pluronic-PLL@Au NPs (Group V) were intravenously injected into MDA-MB-231 tumor-bearing mice; then, the tumors were locally irradiated by an 808-nm NIR laser at a laser power output of 1.0 W/cm² for 2 min at 8 h post-injection. As controls, mice were treated with PBS (Group I), Taxol (Group II), PTX-loaded Pluronic-PLL@Au NPs without laser irradiation (Group III) and Pluronic-PLL@Au NPs with laser irradiation (Group IV). Figure 10A shows the infrared thermal images of the tumor surface in Group I, IV and V mice. During irradiation, a significant temperature increase of 35 °C and 34 °C was found in Pluronic-PLL@Au NPs and PTX-loaded Pluronic-PLL@Au NPs injected tumors, which was high enough to ablate tumors in vivo. In contrast, the tumor temperature in the mouse intravenously injected with PBS under the same irradiation conditions showed little change. Subsequently, tumor volumes and body weight were measured every 3 days for up to 30 days, as shown in Figure 10B-C. On the 30th day, the mice were sacrificed and tumors were excised (Fig. 10D). The PBS and free Taxol groups resulted in a more than 4.7-fold and 3.4-fold increase in average tumor volumes compared to their original volumes, respectively, demonstrating that free Taxol had a slight therapeutic efficacy. Group V exhibited the slowest tumor growth behaviors compared to Group III ($P<0.05$) and Group IV ($P<0.001$), suggesting a synergistic tumor growth inhibition effect between PTX-loaded Pluronic-PLL@Au NP treatment and laser irradiation. The result that the drug delivery system is more efficient than Taxol is due to several key factors. First, drug-loaded Pluronic-PLL@Au NPs can be more easily gathered at the tumor site compared with the free drug because of the EPR effect. Second, the positively charged drug-loaded Pluronic-PLL@Au NPs enhanced the cellular uptake efficiency. The diffusion of the free small drug molecule depends on the concentration gradient. In addition, the body weight measurement showed that the weight of all groups increased, except for that of Group II. These results suggested that PTX-loaded Pluronic-PLL@Au NPs are a promising agent for *in vivo* chemo-photothermal therapy without causing obvious toxicity conditions. In Fig. 10E, images of hematoxylin and eosin (H&E)-stained tumor from the MDA-MB-231 tumor-bearing mice show more severe cancer necrosis in the PTX-loaded Pluronic-PLL@Au NPs with laser irradiation group compared with other groups. In addition, there is no remarkable damage to the heart, liver, spleen, lung, or kidney of MDA-MB-231 tumor-bearing mice with different treatments (Figure S7). These results demonstrated that PTX-loaded Pluronic-PLL@Au NPs with laser irradiation can make a significant advance in cancer therapy with low side effects on normal tissues.

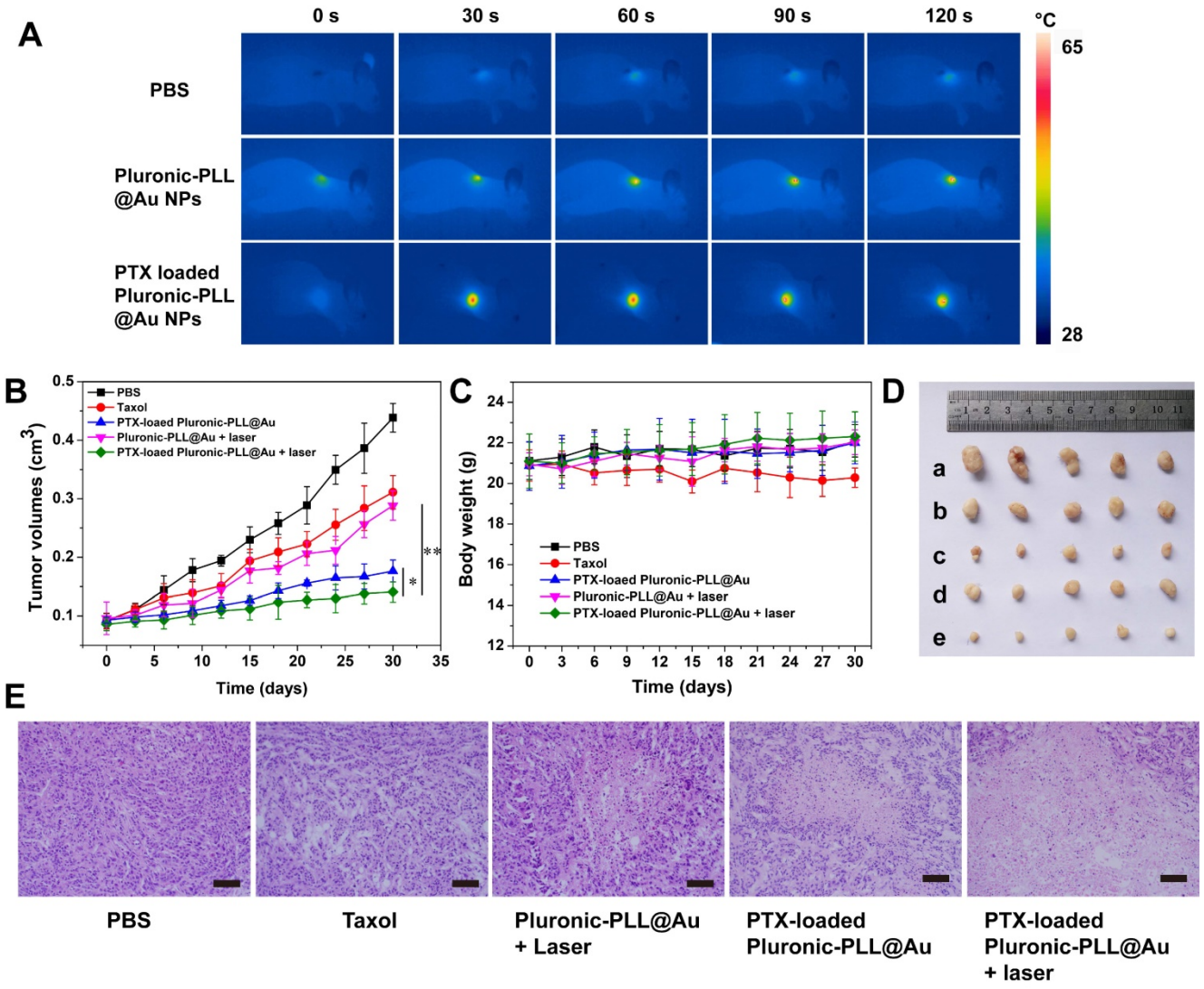

Figure 10. *In vivo* chemo-photothermal therapy. (A) The infrared thermal image of tumor-bearing mice under an 808-nm NIR laser irradiation at 8 h post intravenous injection of PBS, Pluronic-PLL@Au NPs and PTX-loaded Pluronic-PLL@Au NPs with 1 W/cm² for 120 s. (B) Tumor growth and (C) body weight of MDA-MB-231 breast cancer-bearing mice after various treatments. Groups were given PBS, Taxol, Pluronic-PLL@Au NPs with laser irradiation, PTX-loaded Pluronic-PLL@Au NPs without laser irradiation and PTX-loaded Pluronic-PLL@Au NPs with laser irradiation. The data are presented as the mean ± S.D. (n = 5). *$p < 0.05$, **$p < 0.001$. (D) Photographs of tumors with different treatments: a) PBS, b) Taxol, c) PTX-loaded Pluronic-PLL@Au NPs without laser irradiation, d) Pluronic-PLL@Au NPs with laser irradiation, and e) PTX-loaded Pluronic-PLL@Au NPs with laser irradiation. (E) Images of H&E-stained tumor from the MDA-MB-231 tumor-bearing mice with different treatments (scale bar = 100 μm).

Conclusion

In summary, block copolymer Pluronic-PLL was synthesized by the deprotection of Pluronic-PZLL that was prepared through ROP of ZLys NCA with Pluronic-NH_2 used as a macroinitiator. We have developed an easy one-step strategy to synthesize Pluronic-PLL@Au NPs capped with positively charged PLL. This method for the preparation of Pluronic-PLL@Au NPs was considered to be a green approach because of the use of Pluronic-PLL as both the reducing agent and the stabilizing agent. The preparation process does not require an additional reducing agent or removal of the chemical reagents after post-processing. We fabricated PTX-loaded Pluronic-PLL@Au NPs that can be simultaneously used as a drug delivery carrier for chemotherapy and photothermal therapy.

Overall studies were carried out on the treatment of tumors *in vitro* and *in vivo*. PTX-loaded nanoparticles induced a higher cytotoxicity compared to Taxol. Chemo-photothermal co-therapy caused a synergistic effect, and the co-therapeutic efficacies were higher than the additive therapeutic efficacy of chemo- and photothermal therapy. These results implied the potential of PTX-loaded Pluronic-PLL@Au NPs in combined chemotherapy and photothermal therapy for the clinical treatment of breast cancers.

Supplementary Material

Supplementary figures.
http://www.thno.org/v07p4424s1.pdf

Abbreviations

FDA: Food and Drug Administration; PEO-PPO-PEO: poly(ethylene oxide)-poly(propylene oxide)-poly(ethylene oxide); CMC: critical micelle concentration; PLL: Poly(L-lysine); Pluronic-PLL: Pluronic-b-poly(L-lysine); PTX: paclitaxel; RB: Rhodamine B.

Acknowledgments

This research was supported by the National Natural Science Foundation of China (No. 81472841, No. 81572999, No. 81502692, No. 81602718, No. 81771839 and No. 81773272), the State Key Laboratory of Oncogenes and Related Genes (No. 91-17-02), the Three-year (2014-2016) Action Plan for Further Development of Traditional Chinese Medicine of Shanghai (No. ZY3-CCCX-3-3032) and the Shanghai Municipal Health and Family Planning Commission Foundation (No. 201440015).

Competing Interests

The authors have declared that no competing interest exists.

References

1. Liu HL, Jablonska A, Li YG, Cao SY, Liu DX, Chen HW, Zijl P, Bulte J, Janowski M, Walczak P, Liu GH. Label-free CEST MRI Detection of Citicoline-Liposome Drug Delivery in Ischemic Stroke. Theranostics. 2016; 6: 1588-1600.
2. Tanaka T, Decuzzi P, Cristofanilli M, Sakamoto JH, Tasciotti E, Robertson FM, Ferrari M. Nanotechnology for Breast Cancer Therapy. Biomed Microdevices. 2009, 11: 49-63.
3. Dong ZL, Gong H, Gao M, Zhu WW, Sun XQ, Feng LZ, Fu TT, Li YG, Liu Z. Polydopamine Nanoparticles as a Versatile Molecular Loading Platform to Enable Imaging-guided Cancer Combination Therapy. Theranostics. 2016, 6: 1031-1042.
4. Cheng TJ, Liu JJ, Ren J, Huang F, Ou HL, Ding YX, Zhang YM, Ma RJ, An YL, Liu JF, Shi LQ. Green Tea Catechin-Based Complex Micelles Combined with Doxorubicin to Overcome Cardiotoxicity and Multidrug Resistance. Theranostics. 2016; 6: 1277-1292.
5. Almeida H, Amaral MH, Lobao P, Lobo JMS. In situ gelling systems: a strategy to improve the bioavailability of ophthalmic pharmaceutical formulations. Drug Discov Today. 2014; 19: 400-412.
6. Powell KC, Damitz R, Chauhan A. Relating emulsion stability to interfacial properties for pharmaceutical emulsions stabilized by Pluronic F68 surfactant. Int J Pharm. 2017; 521: 8-18.
7. Xu JP, Yang X, Lv LP, Wei Y, Xu FM, Ji J. Gold-Nanoparticle-Stabilized Pluronic Micelles Exhibiting Glutathione Triggered Morphology Evolution Properties. Langmuir. 2010; 26: 16841-16847.
8. Shukla SC, Amit S, Anand KP, Abha M. Review on production and medical applications of ε-polylysine. Biochem Eng J. 2012; 65: 70-81.
9. Yan X, Blacklock J, Li J, Mohwald H. One-Pot Synthesis of Polypeptide-Gold Nanoconjugates for in Vitro Gene Transfection. ACS Nano. 2012; 6: 111-117.
10. Chen HL, Liu Zm, Li SY, Su CK, Qiu XJ, Zhong HQ, Guo ZY. Fabrication of Graphene and AuNP Core Polyaniline Shell Nanocomposites as Multifunctional Theranostic Platforms for SERS Real-time Monitoring and Chemo-photothermal Therapy. Theranostics. 2016; 6: 1096-1104.
11. Giljohann DA, Seferos DS, Daniel WL, Massich MD, Patel PC, Mirkin CA. Gold Nanoparticles for Biology and Medicine. Angew Chem Int Edit. 2010; 49: 3280-3294.
12. Jing LJ, Liang XL, Li XD, Lin L, Yang YB, Yue XL, Dai ZF. Mn-porphyrin Conjugated Au Nanoshells Encapsulating Doxorubicin for Potential Magnetic Resonance Imaging and Light Triggered Synergistic Therapy of Cancer. Theranostics. 2014; 4: 858-871.
13. Stobiecka M, Hepel M. Double-Shell Gold Nanoparticle-Based DNA-Carriers with Poly-L-Lysine Binding Surface. Biomaterials. 2011; 32: 3312-3321.
14. Chen J, Wang D, Xi J, Au L, Siekkinen A, Warsen A, Li ZY, Zhang H, Xia Y, Li X. Immuno Gold Nanocages with Tailored Optical Properties for Targeted Photothermal Destruction of Cancer Cells. Nano Lett. 2007; 7: 1318-1322.
15. Park H, Yang J, Lee J, Haam S, Choi IH, Yoo KH. Multifunctional Nanoparticles for Combined Doxorubicin and Photothermal Treatments. ACS Nano. 2009; 3: 2919-2926.
16. Tong L, Zhao Y, Huff TB, Hansen MN, Wei A, Cheng JX. Gold Nanorods Mediate Tumor Cell Death by Compromising Membrane Integrity. Adv Mater. 2007; 19: 3136-3141.
17. Astruc D, Daniel MC. Gold Nanoparticles: Assembly, Supramolecular Chemistry, Quantum-Size-Related Properties, and Applications toward Biology, Catalysis, and Nanotechnology Epilepsia. Chem Rev. 2004; 104: 293-346.
18. Koo YS, Kazemi R, Liu QH, Philips JC, Fathy AE. Development of a High SAR Conformal Antenna for Hyperthermia Tumors Treatment. IEEE T Antenn Propag. 2014; 62: 5930-5840.
19. Daly WH, Poché D. The Preparation of N-Carboxyanhydrides of α-amino Acids Using Bis(trichloromethly) Carbonate. Tetrahedron Letters. 1988; 29: 5859-5862.
20. Yu H, Gu XH, Shen XY, Li YG, Duan YR. Synthesis and Characterization of Biodegradable Block Copolymer Pluronic-b-poly(L-Lysine). J Appl Polym Sci. 2009; 112: 3371-3379.
21. Deng C, Chen XS, Yu HJ, Sun J, Lu TC, J XB. A biodegradable triblock copolymer poly(ethylene glycol)-bpoly(L-lactide)-b-poly(L-lysine): Synthesis, self-assembly, and RGD peptide modification. Polymer. 2007; 48: 139-149.
22. Ma YK, Fan XH, Li LB. pH-sensitive polymeric micelles formed by doxorubicin conjugated prodrugs for co-delivery of doxorubicin and paclitaxel. Carbohydr Polym. 2016; 137: 19-29.
23. Teng YW, Shen X, Zheng LM, Gong T, Sun Y, Duan YR. Synthesis of Gold-Nanoshelled Pluronic-PEI Nanocapsules for Drug Delivery. J Nanosci Nanotechno. 2016; 16: 12154-12160.
24. Han LM, Guo J, Zhang LJ, Wang QS, Fang XL. Pharmacokinetics and Biodistribution of Polymeric Micelles of Paclitaxel with Pluronic P123. Acta Pharmacol Sin. 2006; 27: 747-753.
25. Wang QZ, Chen XG, Li ZX, Wang S, Liu CS, Meng XH, Liu CG, Lv YH, Yu LJ. Preparation and blood coagulation evaluation of chitosan microspheres. J Mater Sci-Mater M. 2008; 19: 1371-1377.
26. Zhang E, Chen HY, Shen F. Biocorrosion properties and blood and cell compatibility of pure iron as a biodegradable biomaterial. J Mater Sci-Mater M. 2010; 21: 2151-2163.
27. Muzzarelli RAA, Guerrieri M, Goteri G, Muzzarelli C, Armeni T, Ghiselli R, Cornelissen M. The biocompatibility of dibutyryl chitin in the context of wound dressings. Biomaterials. 2005; 26: 5844-5854.
28. Wang Q, Liu PF, Sun Y, Gong T, Zhu MJ, Sun X, Zhang ZY, Duan YR. Preparation and properties of biocompatible PS-PEG/calcium phosphate nanospheres. Nanotoxicology. 2015; 9: 1-11.
29. Lin D, Huang Y, Jiang Q, Zhang W, Yue X, Guo S, Xiao P, Du Q, Xing J, Deng L, Liang Z, Dong A. Structural Contributions of Blocked or Grafted Poly(2-dimethylaminoethyl methacrylate) on PEGylated Polycaprolactone Nanoparticles in SiRNA Delivery. Biomaterials. 2011; 32: 8730-8742.
30. Deng C, Chen XS, Sun J, Lu TC, Wang WS, Jing XB. RGD peptide grafted biodegradable amphiphilic triblock copolymer poly(glutamic acid)-b-poly(L-lactide)-b-poly(glutamic acid): Synthesis and self-assembly. J Polym Sci Pol Chem. 2007; 45: 3218-3230.
31. Deng C, Tian H, Zhang P, Sun J, Chen X, Jing X. Synthesis and Characterization of RGD Peptide Grafted Poly(ethylene glycol)-b-Poly(L-lactide)-b-Poly(L-glutamic Acid) Triblock Copolymer. Biomacromolecules. 2006; 7: 590-596.
32. Zhu MQ, Xiang L, Yang K, Shen LJ, Long F, Fan JB, Yi HQ, Xiang J, Aldred MP. Synthesis and characterization of biodegradable amphiphilic triblock copolymers methoxy-poly(ethylene glycol)-b-poly (L-lysine)-b-poly(L-lactic acid). J Polym Res. 2012; 19: 9808.
33. Rejman J, Oberle V, Zuhorn IS, Hoekstra D. Size-Dependent Internalization of Particles via the Pathways of Clathrin- and Caveolae-Mediated Endocytosis. Biochem J. 2004; 377: 159-169.
34. Zhang W, Gilstrap K, et al. Synthesis and Characterization of Thermally Responsive Pluronic F127-Chitosan Nanocapsules for Controlled Release and Intracellular Delivery of Small Molecules. ACS Nano. 2010; 4: 6747-6759.
35. Huang H, Yang X. Synthesis of Chitosan-Stabilized Gold Nanoparticles in the Absence/Presence of Tripolyphosphate. Biomacromolecules. 2004; 5: 2340-2346.
36. Liu LW, Yong KT, Roy I, Law WC, Ye L, Liu JW, Liu J, Kumar R, Zhang XH, Prasad PN. Bioconjugated Pluronic Triblock-Copolymer Micelle-Encapsulated Quantum Dots for Targeted Imaging of Cancer: In Vitro and In Vivo Studies. Theranostics. 2012; 2: 705-713.
37. Bae KH, Choi SH, Park SY, Lee Y, Park TG. Thermosensitive Pluronic Micelles Stabilized by Shell Cross-Linking with Gold Nanoparticles. Langmuir. 2006; 22: 6380-6384.
38. Chen HY, Zhang X, Dai SH, Ma YX, Cui SS, Achilefu S, Gu YQ. Multifunctional Gold Nanostar Conjugates for Tumor Imaging and Combined Photothermal and Chemotherapy. Theranostics. 2013; 3: 633-649.
39. Ke H, Wang J, Dai Z, Jin Y, Qu E, Xing Z, Guo C, Yue X, Liu J. Gold-Nanoshelled Microcapsules: a Theranostic Agent for Ultrasound

Contrast Imaging and Photothermal Therapy. Angew Chem Int Edit. 2011; 50: 3017-3021.
40. Hu J, Zhu XL, Li H, Zhao ZH, Chi XQ, Huang GM, Huang DT, Liu G, Wang XM, Gao JH. Theranostic Au cubic nano-aggregates as potential photoacoustic contrast and photothermal therapeutic agents. Theranostics. 2014; 4:534-545.
41. ISO-10993-4. Biological Evaluation of Medical Devices-Part 4: Selection of Tests for Interactions with blood. Arlington: ANSI/AAMI. 1999.
42. Autian J. Biological model systems for the testing of the toxicity of biomaterials. Polymers in medicine and surgery. In: Kronenthal RL, Oser Z, Martin E, editors. Polymer science and technology. New York: Plenum Press; 1975: 181-203.
43. Braut-Boucher F, Pichon J, Rat P, Adolphe M, Aubery M, Font J. A Non-Isotopic, Highly Sensitive, Fluorimetric, Cell-Cell Adhesion Microplate Assay using Calcein AM-Labeled Lymphocytes. J Immunol Methods. 1995; 178: 41-51.
44. Osaka T, Nakanishi T, Shanmugam S, Takahama S, Zhang H. Effect of surface charge of magnetite nanoparticles on their internalization into breast cancer and umbilical vein endothelial cells. Colloid Surface B. 2009; 71: 325-330.
45. Lamprecht A, Benoit JP. Etoposide nanocarriers suppress glioma cell growth by intracellular drug delivery and simultaneous P-glycoprotein inhibition. J Control Release. 2006; 112: 208-213.